Since January 2020 Elsevier has created a COVID-19 resource centre with free information in English and Mandarin on the novel coronavirus COVID-19. The COVID-19 resource centre is hosted on Elsevier Connect, the company's public news and information website.

Article

Cell Reports

Cellular Importin-α3 Expression Dynamics in the Lung Regulate Antiviral Response Pathways against Influenza A Virus Infection

Graphical Abstract

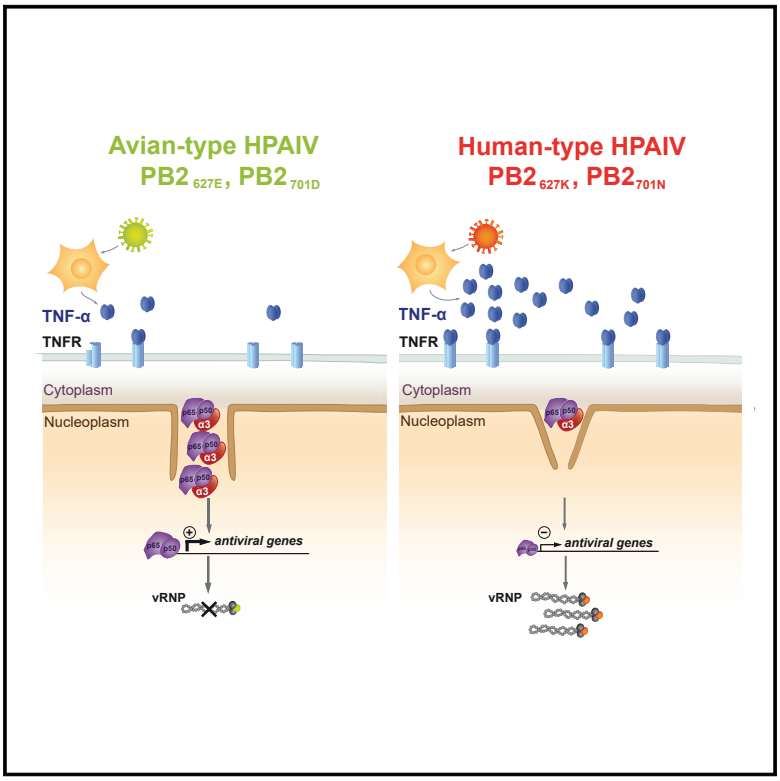

Highlights

- Importin-α3 is the most abundantly expressed isoform in the mammalian lung
- Importin-α3 is highly conserved across species
- Importin-α3 is one of the major nuclear transporters of NF-κB
- Importin-α3 acts as an immune sensor of influenza A virus infections

Authors

Swantje Thiele, Stephanie Stanelle-Bertram, Sebastian Beck, ..., Michael Bader, Enno Hartmann, Gülsah Gabriel

Correspondence

guelsah.gabriel@leibniz-hpi.de

In Brief

Thiele et al. show that importin-α3 is one of the major nuclear transporters of NF-κB in the mammalian lung. High-level TNF-α-inducing HPAIVs inhibit importin-α3 mRNA transcription by interfering with its promoter activity. Thus, HPAIVs may evade antiviral immunity in the respiratory tract by generating a bottleneck in importin-α3 availability.

Thiele et al., 2020, Cell Reports *31*, 107549
April 21, 2020
https://doi.org/10.1016/j.celrep.2020.107549

CellPress

Cell Reports
Article

Cellular Importin-α3 Expression Dynamics in the Lung Regulate Antiviral Response Pathways against Influenza A Virus Infection

Swantje Thiele,[1] Stephanie Stanelle-Bertram,[1] Sebastian Beck,[1] Nancy Mounogou Kouassi,[1] Martin Zickler,[1] Martin Müller,[1] Berfin Tuku,[1] Patricia Resa-Infante,[1,12] Debby van Riel,[1,3] Malik Alawi,[4,5] Thomas Günther,[5] Franziska Rother,[6,7] Stefanie Hügel,[6] Susanne Reimering,[8] Alice McHardy,[8] Adam Grundhoff,[5] Wolfram Brune,[9] Albert Osterhaus,[10] Michael Bader,[6,7,11] Enno Hartmann,[7] and Gülsah Gabriel[1,2,13,*]

[1]Viral Zoonosis – One Health, Heinrich Pette Institute, Leibniz Institute for Experimental Virology, Hamburg, Germany
[2]Institute of Virology, University of Veterinary Medicine, Hannover, Germany
[3]Department of Viroscience, Erasmus Medical Center, Rotterdam, the Netherlands
[4]Bioinformatics Service Facility, University Medical Center Hamburg-Eppendorf, Hamburg, Germany
[5]Virus Genomics, Heinrich Pette Institute, Leibniz Institute for Experimental Virology, Hamburg, Germany
[6]Molecular Biology of Peptide Hormones, Max Delbrück Center for Molecular Medicine, Berlin, Germany
[7]Institute for Biology, Center for Structural and Cellular Biology in Medicine, University of Lübeck, Lübeck, Germany
[8]Computational Biology of Infection Research, Helmholtz Centre for Infection Research, Braunschweig, Germany
[9]Virus-Host Interaction, Heinrich Pette Institute, Leibniz Institute for Experimental Virology, Hamburg, Germany
[10]Research Center for Emerging Infections and Zoonoses, University of Veterinary Medicine Hannover, Hannover, Germany
[11]Charité-Universitätsmedizin, Berlin, Germany
[12]Present address: AIDS Research Institute IrsiCaixa, Barcelona, Spain
[13]Lead Contact
*Correspondence: guelsah.gabriel@leibniz-hpi.de
https://doi.org/10.1016/j.celrep.2020.107549

SUMMARY

Importin-α adaptor proteins orchestrate dynamic nuclear transport processes involved in cellular homeostasis. Here, we show that importin-α3, one of the main NF-κB transporters, is the most abundantly expressed classical nuclear transport factor in the mammalian respiratory tract. Importin-α3 promoter activity is regulated by TNF-α-induced NF-κB in a concentration-dependent manner. High-level TNF-α-inducing highly pathogenic avian influenza A viruses (HPAIVs) isolated from fatal human cases harboring human-type polymerase signatures (PB2 627K, 701N) significantly downregulate importin-α3 mRNA expression in primary lung cells. Importin-α3 depletion is restored upon back-mutating the HPAIV polymerase into an avian-type signature (PB2 627E, 701D) that can no longer induce high TNF-α levels. Importin-α3-deficient mice show reduced NF-κB-activated antiviral gene expression and increased influenza lethality. Thus, importin-α3 plays a key role in antiviral immunity against influenza. Lifting the bottleneck in importin-α3 availability in the lung might provide a new strategy to combat respiratory virus infections.

INTRODUCTION

Molecular trafficking of proteins between the cytoplasm and the nucleus is a fundamental process that is essential to maintain cellular homeostasis (Görlich and Mattaj, 1996; Imamoto et al., 1995). Disturbances in these highly sensitive regulatory processes may result in the disequilibrium of cellular and nuclear proteins and eventually cause diseases. Importin-α proteins belong to the major nuclear transport factors in the cell shuttling various cargo proteins containing a nuclear localization signal (NLS) from the cytoplasm to the nucleus (Goldfarb et al., 2004). Importin-α proteins are acidophilic proteins that bind as adaptors to cargo proteins containing a basic stretch of mono- or bipartite NLS motifs. This importin-α/cargo complex forms a trimeric complex with the receptor protein importin-β_1, which finally translocates through the nuclear pore by the interaction of importin-β_1 with nucleoporins (Hu et al., 1996; Radu et al., 1995; Rexach and Blobel, 1995). In the nucleus, the guanosine triphosphate (GTP)-bound form of Ran binds to importin-β_1 and mediates the dissociation and release of the cargo protein into the nucleus (Lee et al., 2005; Matsuura and Stewart, 2005). After successful nuclear import, importin-α binds to the recycling factor cellular apoptosis susceptibility protein (CAS) that, in conjunction with RanGTP, transports the complex back into the cytoplasm where importin-α is again available for the nuclear import of other cargo proteins (Kutay et al., 1997). Importin-α proteins are highly conserved throughout evolution (Goldfarb et al., 2004). In eukaryotes, seven importin-α isoforms were described, whereas the budding yeast encodes one importin-α, and flies and nematodes encode for three importin-α isoforms. However, all of these organisms encode for only one importin-β_1 receptor protein. The specificity of importin-α isoforms to cargo proteins is determined by the complexity and the three-dimensional context (Friedrich et al., 2006; Goldfarb et al., 2004; Sankhala et al., 2017). Moreover, importin-α proteins play a key role in cellular differentiation by regulating the transport of transcription

factors through lineage-specific expression profiles in cells (Yasuhara et al., 2007). However, little is known about the expression profiles of importin-α isoforms in organs that could give important insights into molecular mechanisms in health and disease. There is accumulating evidence that under cellular stress, such as oxidative stress, heat shock, or ultraviolet irradiation, importin-α proteins may accumulate in the nucleus and disrupt cellular homeostasis (Furuta et al., 2004; Kodiha et al., 2004; Yasuda et al., 2012). In the last decade, a growing amount of evidence suggests that importin-α proteins are utilized by various viruses (e.g., influenza, Ebola, dengue, hepatitis C, and coronaviruses) to circumvent host defense mechanisms (Basler and Amarasinghe, 2009; Canton et al., 2018; Fraser et al., 2014; Frieman et al., 2007; Gabriel et al., 2011; Hudjetz and Gabriel, 2012; Kopecky-Bromberg et al., 2007; Neufeldt et al., 2013; Pryor et al., 2007). Little evidence is available on their mode of action in specific organs under inflammatory conditions such as virus infections. In this study, we identified the anatomic expression profile of importin-α isoforms in the mammalian lung and studied their transcriptional regulation and impact on influenza-virus-induced pneumonia using cell culture models, genome-wide transcription analyses, and transgenic mouse models.

RESULTS

Importin-α3 Is the Most Abundantly Expressed Importin-α Isoform in the Mammalian Respiratory Tract

In order to analyze the expression pattern of major importin-α isoforms throughout the mammalian respiratory tract (RT), we anatomically dissected the human and murine RT into an upper part defined by respiratory cells of the nasal concha (URT) and a lower part defined by bronchi and alveoli (LRT). Importin-α1, -α3, and -α5/7 isoforms (*Kpna2*, *Kpna4*, and *Kpna1/6*, respectively) were abundantly expressed in epithelial cells, glands, and macrophages of the human (Figure 1A) as well as the murine URT and LRT (Figure 1B). We then measured the relative mRNA expression levels of importin-α isoforms along the mammalian RT. In the human URT and LRT, importin-α3 was by far the most abundantly expressed isoform, with 4–5 times increased mRNA levels compared to importin-α1. Average expression levels of other isoforms were similar to those of importin-α1, except for importin-α7, which was the second-most abundant isoform (Figure 1C). Similarly, importin-α3 was also the highest-expressed isoform, followed by importin-α7 in the murine URT and LRT. Laser-based microdissection of epithelial cells was used to ensure homogeneous cell populations (Figure 1D). We further confirmed the exclusive abundance of importin-α3 in the murine lung, followed by importin-α7 as the second-most abundant isoform also on the protein level, using whole-organ homogenates (Figures 1E and 1F). Notably, in immortalized cells (Figures S1A–S1D) and unlike in primary cells, importin-α1 is the most abundant isoform and is therefore used as a prognostic cancer marker (Christiansen and Dyrskjøt, 2013; Dahl et al., 2006; Kau et al., 2004). Thus, it is particularly important to investigate the role of importin-α isoforms either in primary cells or in an *in vivo* animal model. We then determined the expression of importin-α isoforms in various murine organs on the mRNA and protein levels and confirmed that the lung (Figure S1E) is unique in exhibiting exclusively high importin-α3 levels, compared to other solid organs (Figures S1F–S1K). Moreover, comparable distribution and expression levels of importin-α isoforms within the human and murine RT suggest that the mouse model may be considered adequate to study the impact and mode-of-action of these cellular factors in health and disease. Next, we directly compared relative importin-α amounts in laser-microdissected epithelial samples of the URT versus the LRT (Figures 1G–1K). For all importin-α isoforms, mRNA levels were highest in the alveolar tissue (LRT (A), up to 6 times) followed by epithelial cells of the bronchi and bronchioles (LRT [bronchiolar epithelium, BE]). The lowest mRNA levels were detected in epithelial cells of the nasal concha (URT). Thus, importin-α isoforms are expressed as a gradient in the RT with gradually increasing mRNA levels from the URT toward the LRT (Figure 1L). However, importin-α3 is the most abundantly expressed importin-α isoform in the mammalian RT, unlike in other solid organs.

Importin-α3 Mediates Nuclear Translocation of TNF-α-Activated NF-κB

NF-κB subunits (p50, p65) are translocated into the nucleus in an importin-α-mediated manner. Herein, particularly importin-α3 and its close relative, importin-α4, were shown to act as one of the main isoforms that imports tumor necrosis factor alpha (TNF-α)-activated p50/p65 heterodimers into the nucleus via direct interaction (Fagerlund et al., 2005). Since the mammalian lung most abundantly expresses the importin-α3 isoform, we continued to dissect the physical and functional interaction between importin-α3 and NF-κB. We could confirm that purified human importin-α3 protein directly interacts with NF-κB p50 and p65 subunits as well as with its precursor p105 protein upon activation with TNF-α unlike importin-α1 that was used as a negative control (Figures 2A and 2B). Consistently, treatment of murine fibroblasts with TNF-α most significantly increased NF-κB levels in nuclear cell fractions along with importin-α3 (Figure 2C). In order to confirm that importin-α3 is required for the nuclear import of NF-κB, we generated murine embryo fibroblasts (MEFs) with a deleted importin-α3 gene ($\alpha3^{-/-}$). Nuclear fractionation analysis in TNF-α-treated $\alpha3^{-/-}$ MEFs showed significantly reduced nuclear translocation of the NF-κB subunit p65 compared to wild-type (WT) control ($\alpha3^{+/+}$) MEFs (Figure 2D). Immunofluorescence analysis further confirmed that nuclear localization of NF-κB p65 was also reduced in $\alpha3^{-/-}$ MEFs compared to $\alpha3^{+/+}$ MEFs (Figure 2E). Conversely, NF-κB p65 accumulated in the cytoplasm of $\alpha3^{-/-}$ MEFs, albeit slightly, likely due to the degradation of inefficiently transported cargo proteins (Figure 2E). The extent of reduced nuclear localization of importin-α3 was dependent on the method used, albeit the absence of importin-α3 consistently impaired efficient nuclear localization of TNF-α-induced NF-κB subunit p65. These data clearly show that importin-α3 acts as a nuclear translocator of TNF-α-activated NF-κB.

Importin-α3 Promoter Activity Is Regulated by TNF-α-Activated NF-κB

We further observed an increase in general importin-α3 protein levels upon TNF-α treatment in total cell lysates, including nuclear and cytoplasmic cell fractions of murine as well as primary

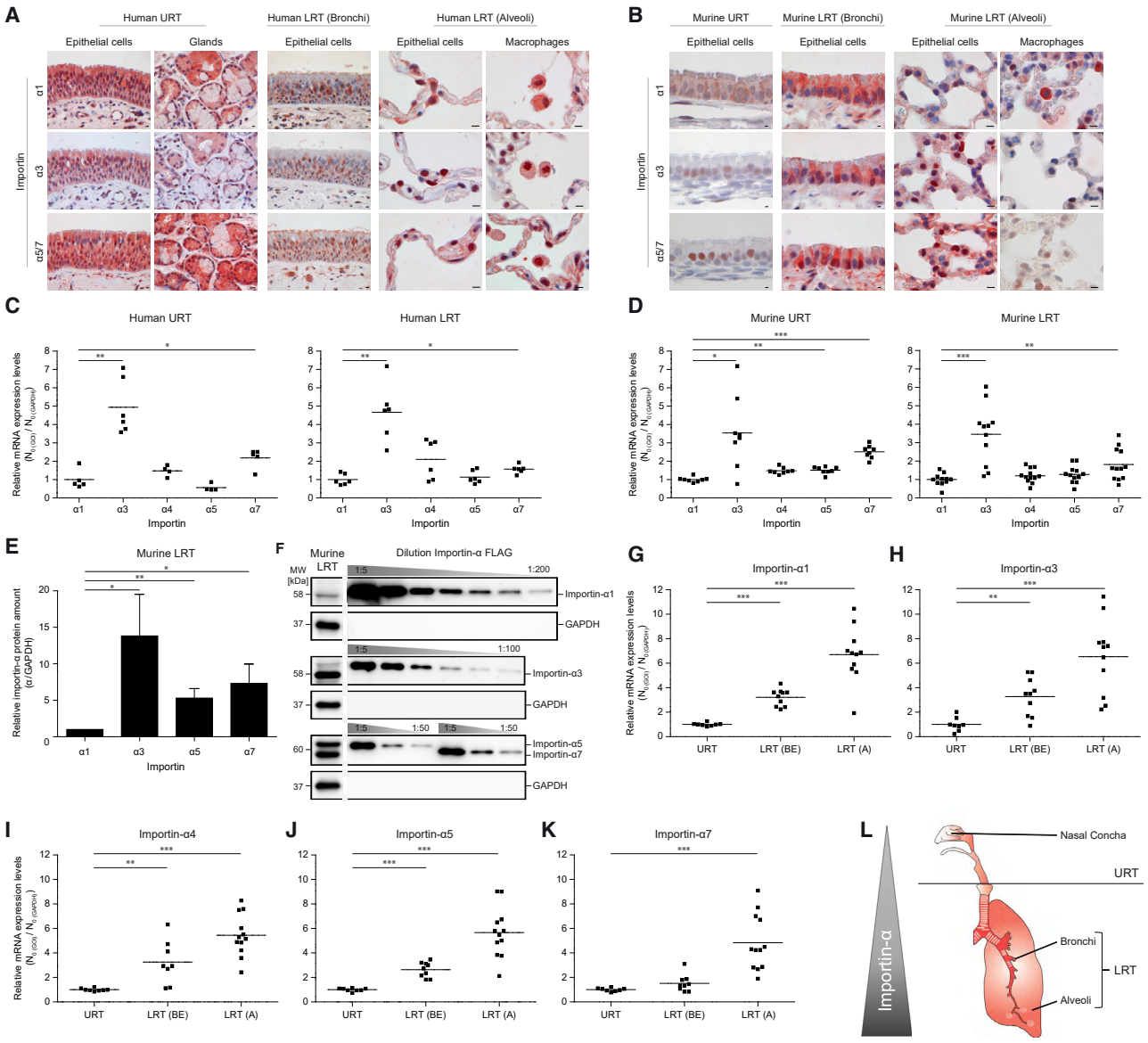

Figure 1. Importin-α Expression in the Mammalian Respiratory Tract

(A and B) Importin-α1, -α3, or -α5/7 proteins were stained (red) in human (A) or murine (B) upper (URT, nasal epithelial cells) and lower respiratory tract (LRT, bronchi and alveoli) sections by IHC-P (immunohistochemistry-paraffin protocol) and counterstained with hematoxylin. The importin-α7 antibody cross-reacts with importin-α5. 400× (URT and bronchi in A) or 1000× (alveoli in A and B) original magnification. Scale bar, 10 μm.

(C and D) Importin-α mRNA levels in the human (C) and murine (D) URT and LRT determined by qRT-PCR. Relative importin-α1 expression values were set to 1 after normalization against GAPDH (Glycerinaldehyd-3-phosphat-dehydrogenase). Each data point represents an individual sample (n = 6–12).

(E and F) Importin-α protein amounts in murine LRT. Western blot analyses using importin-α isoform-specific antibodies and GAPDH adjustment were performed to determine endogenous importin-α protein amounts (α1, α3, α5, α7) in murine organs. For relative quantification (E), standard curves of affinity-purified, FLAG-tagged importin-α proteins were used. Relative importin-α1 protein amount in murine LRT was set to 1. Data shown represent means ± SD (n = 3 biological replicates; technical replicates: n = 1–2 per organ, n = 1–2 western blot analyses). Representative western blots for the endogenous importin-α isoforms and the standard curves are shown in (F). The gaps in (F) depict cropping of the relevant bands run on the same gel.

(G–K) Comparison of importin-α mRNA expression levels between murine URT and LRT: α1 (G), α3 (H), α4 (I), α5 (J), or α7 (K). A, alveoli; BE, bronchiolar epithelium; n = 8–12.

(L) Schematic partition of the RT with increasing importin-α mRNA levels from URT to LRT.

*p < 0.05; **p < 0.01; ***p < 0.001.

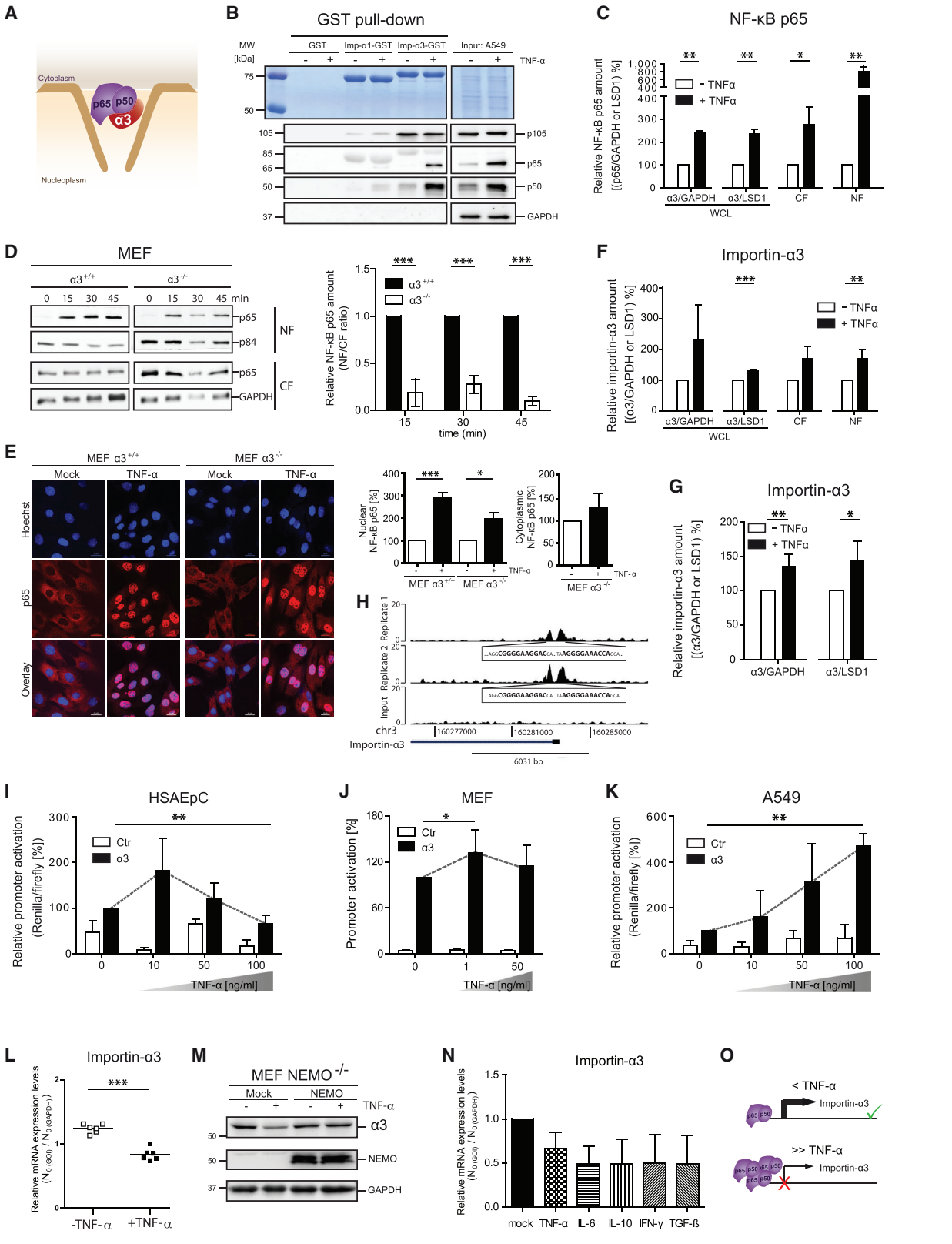

(legend on next page)

airway epithelial cells (Figures 2F and 2G). These findings might suggest that importin-α3 gene expression itself could also be affected by TNF-α treatment. In order to understand how importin-α3 gene transcription is regulated, we screened the promoter region of the importin-α3 gene for the presence of potential transcription factor binding sites. We found that the promoter region of the importin-α3 gene contains a binding site for NF-κB, as shown by earlier chromatin immunoprecipitation studies (Raskatov et al., 2012) (Figure 2H). Consistently, using a reporter construct encoding for renilla luciferase under the control of the importin-α3 promoter, we could show that importin-α3 gene expression is differentially affected upon TNF-α treatment in a cell-type- and dose-dependent manner (Figures 2I–2K). In clinically relevant primary human airway epithelial cells as well as in generated MEFs herein, importin-α3 promoter activity was highest upon low-dose TNF-α treatment, while high-dose TNF-α treatment resulted in a reduction of importin-α3 gene expression (Figures 2J and 2K). However, multi-passage cancerous A549 cells presented high resistance to TNF-α treatment (Figure 2I), suggesting a delayed dose-response curve. Treating MEFs with other cytokines, such as interleukin (IL)-10 or transforming growth factor β (TGF-β) did not significantly alter importin-α3 promoter activity, unlike TNF-α treatment (Figures S2A and S2B), albeit IL-10 presented a slight induction (Figure S2A). Next, we wanted to assess whether TNF-α-activated NF-κB is directly involved in regulating importin-α3 gene transcription. Therefore, we used cells deficient in the NF-κB essential modulator (NEMO), the regulatory subunit of the IKK (IκB kinase), which is required for NF-κB phosphorylation and thus its activation. Importin-α3 mRNA levels were reduced in TNF-α-treated NEMO$^{-/-}$ cells compared to untreated controls (Figure 2L). As expected, reduced importin-α3 mRNA levels also resulted in reduced importin-α3 protein expression in NEMO$^{-/-}$ cells treated with TNF-α as compared to untreated cells (Figure 2M). Reduced importin-α3 expression in NEMO$^{-/-}$ cells could be restored upon transfection of a NEMO-expressing plasmid back into NEMO$^{-/-}$ cells (Figure 2M). Control treatment of NEMO$^{-/-}$ cells with IL-6, IL-10, interferon (IFN)-γ or TGF-β showed similarly reduced importin-α3 mRNA expression levels as upon TNF-α treatment (Figure 2N). It is important to note that IL-6 transcription is directly dependent on NF-κB, unlike IL-10, IFN-γ or TGF-β. These findings support the concept that TNF-α-activated NF-κB is crucial for importin-α3 gene expression. However, other cytokines might also reduce importin-α3 expression at high, but not low, cytokine concentrations (Figure S2C). Our findings support the concept that importin-α3 gene expression is controlled by TNF-α-activated NF-κB in a cell- and dose-dependent manner. This is in line with general control mechanisms in cells, such as negative or positive feedback loops, where gene transcription is regulated (e.g., either by activating or blocking the promoter, respectively, depending on demand) (Figure 2O). However, other, not yet defined, NF-κB-independent pathways might also affect importin-α3 gene expression. Future studies are required to dissect the importin-α3 promotor for transcription factor binding sites other than NF-κB.

High-Level TNF-α-Inducing Human-Type HPAIV Infections Reduce Importin-α3 Protein Expression Levels in Human Respiratory Cells

Since the NF-κB transporting nuclear import factor importin-α3 was the only isoform in the lung that altered its expression levels upon TNF-α treatment, we wanted to know how importin-α3 is regulated under respiratory stress associated with cellular cytokine changes. Therefore, we used an influenza infection model. We infected MEFs with highly pathogenic avian influenza A virus (HPAIV) mutants that were known to act as low- or high-level TNF-α inducers (Figure 3A). Then, we infected MEFs either with the low-level TNF-α-inducing HPAIV containing an avian-type polymerase signature (SC35-PB2$_{701D}$), common in influenza A virus (IAV) having a low replicative fitness in mammals, or its high-level TNF-α-inducing HPAIV counterpart containing a human-type polymerase signature (SC35M-PB2$_{701N}$), common in IAV possessing a high replicative fitness and virulence

Figure 2. Molecular Function and Regulation of Importin-α3

(A) Schematic overview of importin-α3-mediated NF-κB p65 nuclear translocation.

(B) Pull-down of NF-κB from lysates of untreated or TNF-α-treated A549 cells with Sepharose-immobilized GST-importin-α1 and -α3. Expression of GST-importin-α isoforms was verified with Coomassie staining (upper panel), and bound NF-κB p105, p65, and p50 were detected via western blot (lower panel). GAPDH protein detection served as loading control. One representative experiment is shown out of three independent experiments.

(C) Effect of TNF-α treatment on expression and localization of NF-κB p65 and importin-α3 in WT MEFs (n = 3).

(D and E) Nuclear fraction (NF; control p84) and cytoplasmic fraction (CF; control GAPDH) localization of NF-κB p65 in α3$^{-/-}$ MEFs or WT controls thereof (α3$^{+/+}$) after TNF-α treatment using cell fractionation assay (D) or immunofluorescence (E) as well as quantifications thereof (n = 3–5). Scale bar, 20 μm.

(F and G) After seeding, cells were serum starved for 24 h. Subsequently, cells were control treated (w/o) or treated with TNF-α. Endogenous importin-α3 and NF-κB p65 protein levels were detected and quantified for whole-cell lysates (WCLs), CFs and NFs of WT MEFs (n = 3) (F), and WCLs of HSAEpCs (n = 3) (G). Control-treated samples of each fraction were set to 100%.

(H) NF-κB binding sites in the promoter element of the human importin-α3 gene in A549 cells (Raskatov et al., 2012).

(I–K) Effect of TNF-α treatment on importin-α3 promoter activity in HSAEpC (n = 2) (I), MEFs (n = 3) (J), and A549 cells (n = 6) (K) upon control (Ctr) or importin-α3 promoter reporter construct (α3) transfection. Relative importin-α3 promoter activity in control-treated samples was set to 100%.

(L) Importin-α3 mRNA levels in mock or TNF-α-treated MEF NEMO$^{-/-}$ cells (n = 6). Relative expression values of importin-α3 in samples were normalized to GAPDH, and importin-α1 mRNA expression was set to 1. Each data point represents an individual sample.

(M) MEF NEMO$^{-/-}$ cells were transfected with empty plasmid (Mock) or NEMO and untreated or treated with 50 ng TNF-α. Importin-α3 and NEMO protein expression levels were detected (n = 3). GAPDH protein detection served as loading control.

(N) MEF NEMO$^{-/-}$ cells were treated with 10 ng TNF-α, IL-6, IL-10, IFN-γ and TGF-β and importin-α3 mRNA levels were measured as described above (n = 3)

(O) Importin-α3 gene expression is controlled by TNF-α-activated NF-κB in a dose-dependent manner. Low amounts of TNF-α induce activation of NF-κB and high expression of importin-α3 (upper panel). In contrast, high amounts of TNF-α induce high activation of NF-κB and low expression of importin-α3 (lower panel).

Data shown represent means ± SD of at least three independent biological experiments. *p < 0.05; **p < 0.01; ***p < 0.001.

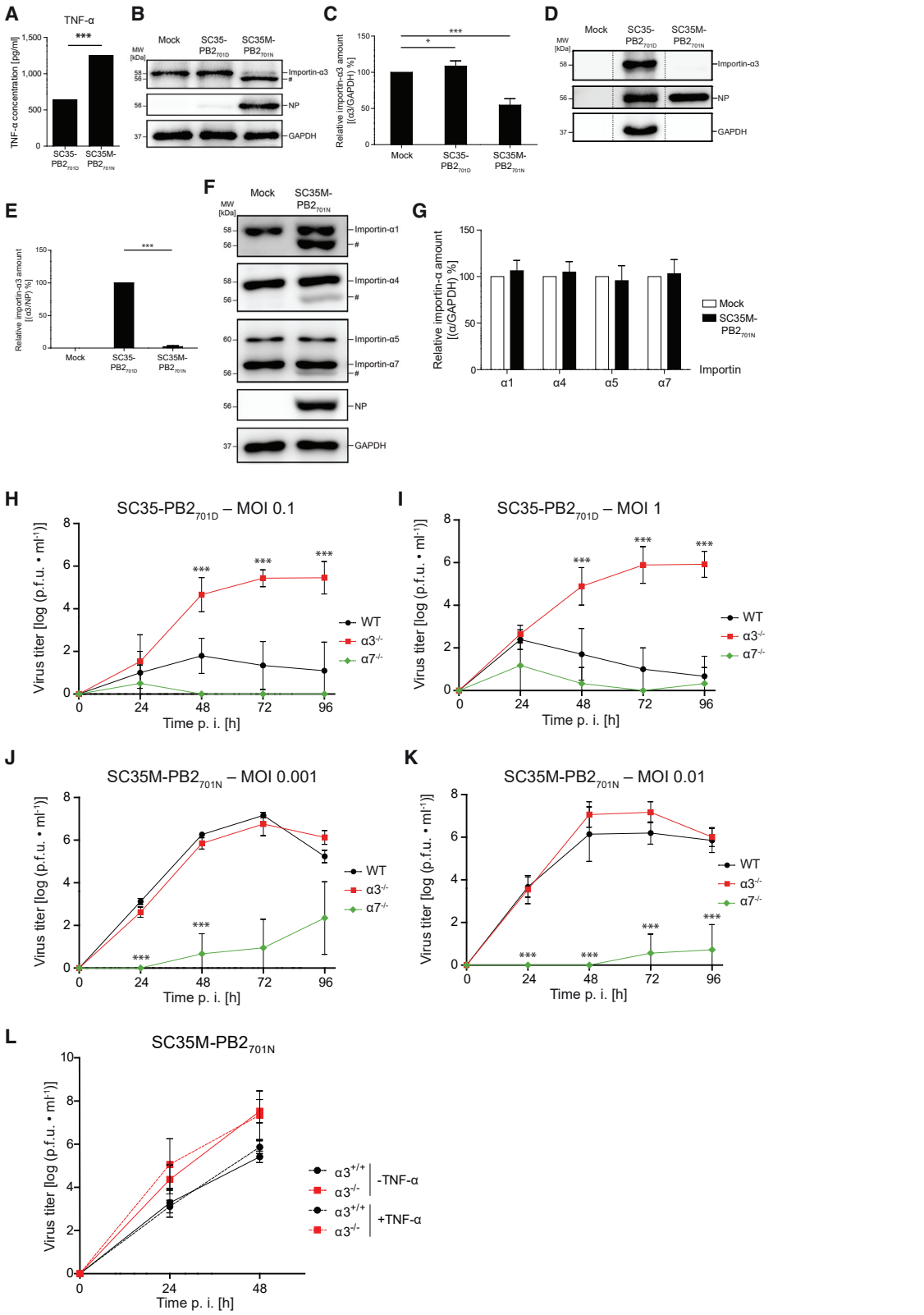

(legend on next page)

in mammalian species. Importin-α3 protein levels were strongly reduced in human-type HPAIV compared to avian-type HPAIV-infected MEFs (Figures 3B–3E). In contrast, protein expression levels of other importin-α isoforms (α1, α4, α5, and α7) were not affected (Figures 3F and 3G). Next, we wanted to assess whether replication of avian- and human-type HPAIV is affected in cells deficient in importin-α3. Cells deficient in importin-α3 were obtained from fibroblasts of mice generated for this study with a deleted importin-α3 gene ($\alpha3^{-/-}$; $\alpha3^{-/-}$ MEFs; Figures S2D and S2E). MEFs with a deficient importin-α7 gene were obtained from mice with a deleted importin-α7 gene ($\alpha7^{-/-}$), described previously (Gabriel et al., 2011). Replication kinetics in MEFs revealed that avian-type but not human-type HPAIV replication is impaired in cells with a deleted importin-α3 gene ($\alpha3^{-/-}$), unlike in control cells, with a deleted importin-α7 gene ($\alpha7^{-/-}$) that acts as a positive factor of human-type HPAIV replication in mammalian cells (Hudjetz and Gabriel, 2012) (Figures 3H and 3I). Interestingly, avian-type HPAIV replication in $\alpha3^{-/-}$ MEFs is increased by >1,000 times compared to WT control cells. Human-type HPAIV replication was comparable between WT and $\alpha3^{-/-}$ cells (Figures 3J and 3K). In line, human-type SC35M-$PB2_{701N}$ HPAIV replication was not affected in human H1299 $\alpha3^{+/+}$ cells upon TNF-α treatment, likely due to the strong inhibition of importin-α3 protein expression (Figure 3L). In human H1299 $\alpha3^{-/-}$ cells, SC35M-$PB2_{701N}$ HPAIV replication slightly increased, suggesting some residual inhibitory activity of importin-α3 in human cells (Figure 3L). These findings show that low-level TNF-α-inducing HPAIVs with avian-type polymerase signatures are highly sensitive to importin-α3-mediated virus restriction. In contrast, high-level TNF-α-inducing HPAIVs with human-type polymerase genes are resistant to importin-α3-mediated virus restriction.

Importin-α3 Belongs to the Most Conserved Nuclear Transport Factors between Avian and Mammalian Species

Differential regulation of importin-α3 expression levels upon avian- and human-type HPAIV infections prompted us to analyze the sequence identity of importin-α isoforms in various avian and mammalian species. Among all importin-α isoforms analyzed, importin-α1 was the most diverse nuclear import factor, with amino acid homology of 83.52% between chicken and humans (Figure 4A; Table S1). The isoforms importin-α3 and importin-α4 displayed the highest amino acid homologies between chicken and humans of 99.04% and 98.08%, respectively (Figures 4B and 4C; Table S1). Importin-α5, -α6, and -α7 presented amino acid homologies between chicken and humans of 95.91%, 94.22%, and 94.4%, respectively (Figures 4D–4F; Table S1). These findings suggest that particularly importin-α3 and importin-α4, both known nuclear transporters of NF-κB (Fagerlund et al., 2005), are highly conserved across species kingdoms. However, importin-α3 is expressed up to ~5-times-higher levels than importin-α4 in the murine and human lung (Figures 1C and 1D), highlighting particularly the importance of importin-α3 in respiratory immune responses. Thus, acquiring the ability to downregulate importin-α3 in the lung might serve as an important basis in avian-mammalian virus transmission. In order to see whether differential importin-α3 regulation is also present in human isolates, we analyzed human-type HPAIV strains that caused poultry outbreaks with human infections in the Netherlands (H7N7) or Thailand (H5N1). Infection of primary lung cultures with cytokine storm, including TNF-α-inducing H5N1 and H7N7 HPAIV isolates with human-type polymerase signatures ($PB2_{627K}$; $PB2_{701N}$), showed significantly reduced importin-α3 expression levels compared to their counterparts with avian-type polymerase signatures ($PB2_{627E}$; $PB2_{701D}$) (Figures 4G and 4H). These findings highlight the crucial role of importin-α3 as a respiratory factor conserved across animal kingdoms in HPAIV interspecies transmission.

Human-Type Polymerase Signatures in HPAIV Mediate Reduced Importin-α3 mRNA Expression Levels in the Murine BE

Next, we wanted to assess whether differential regulation of importin-α3 can also be detected in a murine infection model. Therefore, we assessed importin-α3 expression levels in lung samples of HPAIV-infected WT mice. Infection with avian-type SC35-$PB2_{701D}$ led to increased importin-α3 mRNA levels in the lung compared to uninfected controls on day 3 post infection (p.i.) (Figures 5A and 5B). In contrast, infection with human-type SC35M-$PB2_{701N}$ resulted in significantly reduced importin-α3 mRNA levels (Figure 5C). Since the human-type SC35M HPAIV contains mainly two host adaptive signatures (PB2 701N and NP 319K), we analyzed recombinant viruses with these single mutations to dissect their individual impact on the dysregulation of importin-α mRNA transcription. Herein, the PB2 D701N host adaptive mutation was predominantly responsible for reduced importin-α3 transcription, while its effect was further enhanced when combined with the NP N319K host

Figure 3. HPAIV Replication Kinetics in Importin-$\alpha3^{-/-}$ Cells

(A) TNF-α induction in MEFs infected with avian-type SC35-$PB2_{701D}$ or human-type SC35M-$PB2_{701N}$ H7N7 HPAIV (MOI = 0.1) measured by ELISA (n = 3).

(B–E) Protein extracts thereof were analyzed and quantified by western blot at 48 h p.i. Importin-α3 and viral NP protein were detected (B and D) and quantified (C and E) with GAPDH (B and C) or NP adjustment (D and E) (n = 4). Dashed lines in (D) depict cropping of the relevant bands run on the same gel.

(F and G) Additionally, importin-α1, -α4, -α5, and -α7 and viral NP protein were detected and quantified with GAPDH adjustment to confirm that observed effects were specific for importin-α3. Control-treated, uninfected samples or SC35-$PB2_{701D}$-infected samples were set to 100%. Cross-reactivity of importin-α antibodies with NP resulted in a band (#) in (B) and (F).

(H–K) Growth kinetics of avian-type SC35-$PB2_{701D}$ (H and I) and human-type SC35M-$PB2_{701N}$ (J and K) H7N7 HPAIV in importin-$\alpha^{-/-}$ MEFs (n = 3). WT (black), importin-$\alpha3^{-/-}$ ($\alpha3^{-/-}$, red), and importin-$\alpha7^{-/-}$ ($\alpha7^{-/-}$, green) MEFs were infected with low (H and J) or high (I and K) multiplicities of infection (MOI). Virus titers given in plaque-forming units (p.f.u.) were determined by plaque assay on MDCKII cells (0, 24, 48, 72, and 96 h p.i.).

(L) H1299 $\alpha3^{+/+}$ (black) and $\alpha3^{-/-}$ (red) cells were infected with human-type SC35M-$PB2_{701N}$ HPAIV (MOI = 0.001) and replication kinetics measured in the presence or absence of TNF-α (n = 3). Virus titers were determined by plaque assay on MDCKII cells (0, 24, 48 h p.i.). Data shown represent means of relative importin-α amounts or logarithmic virus titers ± SD of at least three independent biological experiments (*$p < 0.05$; ***$p < 0.001$).

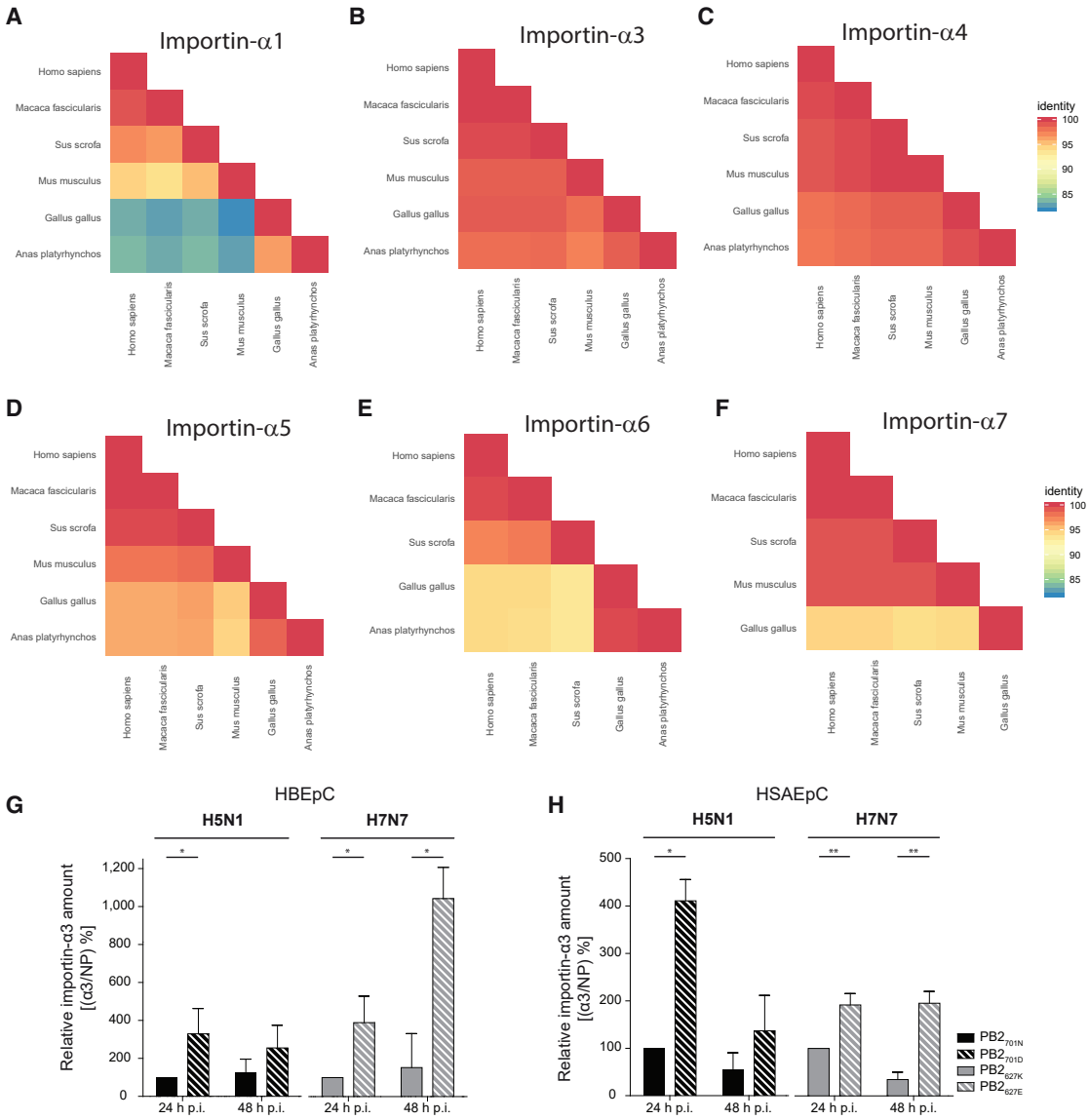

Figure 4. High Importin-α3 Homology across Species and Its Role in HPAIV Interspecies Transmission from Birds to Humans

(A–F) Importin-α homologies across animal kingdoms. Homolgies for importin-α1 (A), -α3 (B), -α4 (C), -α5 (D), -α6 (E), and -α7 (F). Pairwise amino acid sequence identities were calculated for importin-α across species.

(G and H) Primary human bronchial (HBEpC; G) or primary human small airway epithelial cells (HSAEpC; H) were infected with clinical fatal case A/Thailand/1(KAN-1)/2004 (H5N1, MOI = 1) or A/Netherlands/219/2003 (H7N7, MOI = 10) isolates harboring the original human-type signatures ($PB2_{701N}$ or $PB2_{627K}$, respectively) or their recombinant avian-type counterparts ($PB2_{701D}$ or $PB2_{627E}$, respectively). Importin-α3 was quantified in NP-adjusted western blots of HBEpC (H) and HSAEpC (I) infected with H5N1 (MOI = 0.1) or H7N7 (MOI = 1). Importin-α3/NP ratios of human-type virus infected samples at 24 h p.i. were set to 100%. Data shown represent means ± SD of at least three independent biological experiments. *$p < 0.05$; **$p < 0.01$; ***$p < 0.001$.

adaptive signature (Figures 5D–5F). Compared to all other importin-α isoforms, importin-α3 continuously showed the most prominent alterations. Interestingly, the most significant alterations in importin-α3 mRNA levels were detected at 3 days p.i. compared to 1 day p.i. (Figures S2F–S2K), consistent with the concept that accumulating cytokine levels through multiple replication kinetics is required for a profound cytokine-dependent repression of importin-α3 transcription. Avian-type SC35-$PB2_{701D}$ virus replication, which caused an increase in importin-α3 mRNA levels, was restricted to the respiratory tract (Figures S3A and S3B). In contrast, human-type SC35M-$PB2_{701N}$ viral replication led to a significant reduction of importin-α3 mRNA levels in the lung, increased virus load in the lung, and systemic virus spread (Figure S3C). The recombinant viruses with the single or combined human-type PB2 701N and NP 319K signatures showed stepwise systemic spread along with their ability to reduce importin-α3 mRNA levels in the lung (Figures S3D–S3F). These findings further highlight that host

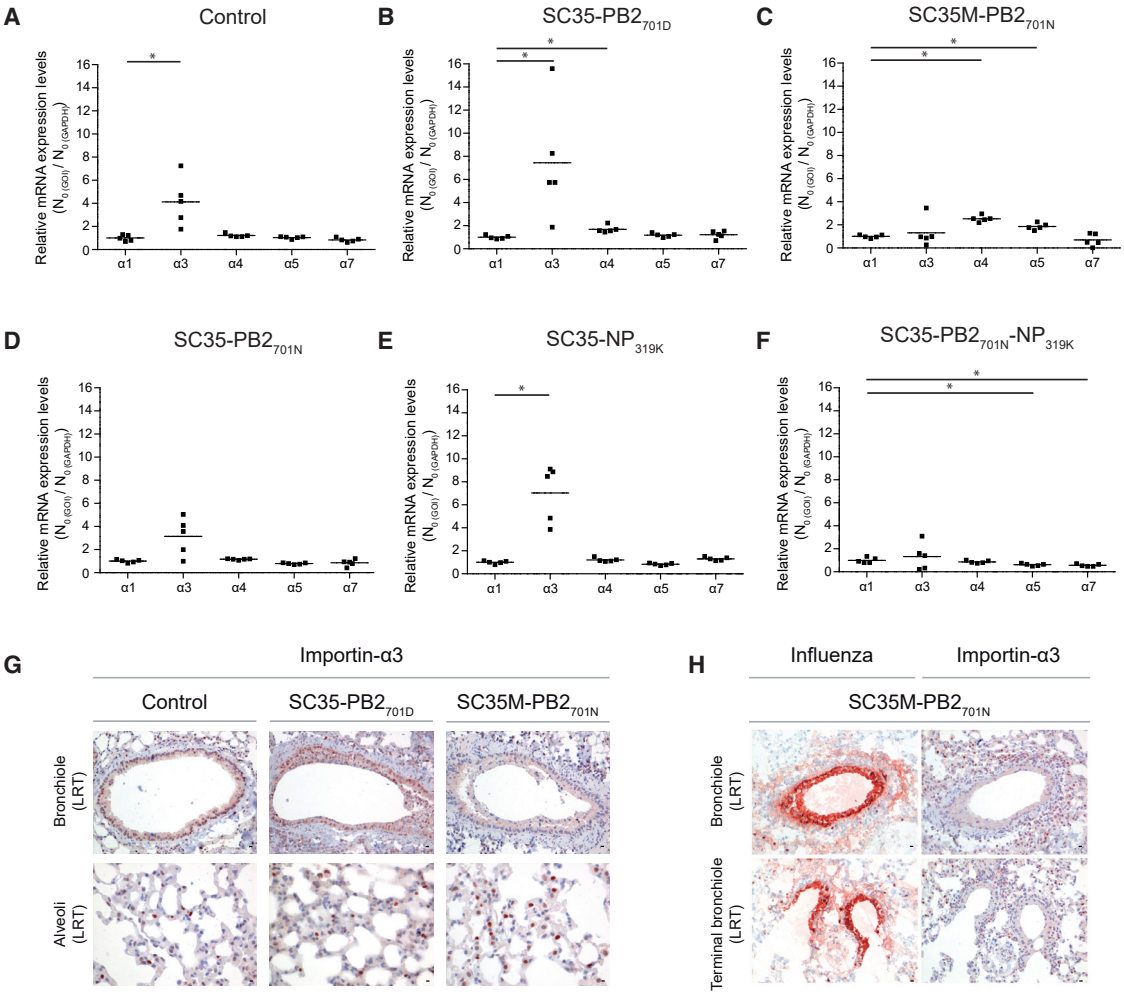

Figure 5. Importin-α3 Expression and Downregulation in Murine Lungs

(A–F) WT mice were control treated or infected with 6×10^4 p.f.u. of H7N7 recombinant viruses. Importin-α mRNA expression levels (α1, α3, α4, α5, α7) on day 3 p.i. in lungs upon control treatment (A) or infection with SC35-PB2$_{701D}$ (B), SC35M-PB2$_{701N}$ (C), SC35-PB2$_{701N}$ (D), SC35-NP$_{319K}$ (E), or SC35-PB2$_{701N}$-NP$_{319K}$ (F) viruses. Relative importin-α1 expression values were set to 1 after normalization against GAPDH. Each data point represents an individual sample (n = 5, *$p < 0.05$).

(G and H) Immunohistochemical staining of importin-α3 (G) and viral antigen (H) on day 3 p.i. in the LRT upon infection with H7N7 HPAIV. 400× original magnification. Scale bar, 10 μm. Immunohistochemical staining of virus antigen (red-brown) in the URT and LRT in α3$^{-/-}$ mice or their WT litters α3$^{+/+}$ infected with 6×10^4 p.f.u. of SC35-PB2$_{701D}$ or SC35M-PB2$_{701N}$ viruses on day 3 p.i. Control mice received PBS.

adaptive signatures mediate impaired importin-α3 transcription, resulting in high-level virus replication.

To determine the respiratory cell types, where reduction of importin-α3 expression occurs, we stained serial lung sections for importin-α3 as well as influenza virus antigen. Importin-α3 was strongly expressed in the BE of avian-type SC35-PB2$_{701D}$-infected mice, correlating with reduced virus-antigen-positive cells in these tissues compared to human-type SC35M-PB2$_{701N}$-infected animals (Figures 5G and 5H). In contrast, importin-α3 protein levels in SC35M-PB2$_{701N}$-infected mice were predominantly reduced in the BE, which correlated with high-level viral replication (Figures 5G and 5H). In line, virus replication was increased in the lungs of α3$^{-/-}$ mice compared to their α3$^{+/+}$ WT littermates infected either with SC35-PB2$_{701D}$ or SC35M-PB2$_{701N}$ virus (Figure S4). Thus, differential regulation of importin-α3 protein expression predominantly occurs in the BE, the key site of productive influenza virus replication (Abdel-Ghafar et al., 2008; Peiris et al., 2007).

Failure to Induce NF-κB-Controlled Antiviral Gene Expression in the Lung Leads to Increased Mortality in Importin-α3-Deficient Mice

Next, we addressed the question of whether reduction of pulmonary importin-α3 levels would affect NF-κB-mediated antiviral gene expression and whether this would affect disease outcome. Therefore, we infected α3$^{-/-}$ mice and their WT litter mates (α3$^{+/+}$) with avian- or human-type HPAIV. Lung transcriptomics of mice infected with human-type SC35M-PB2$_{701N}$

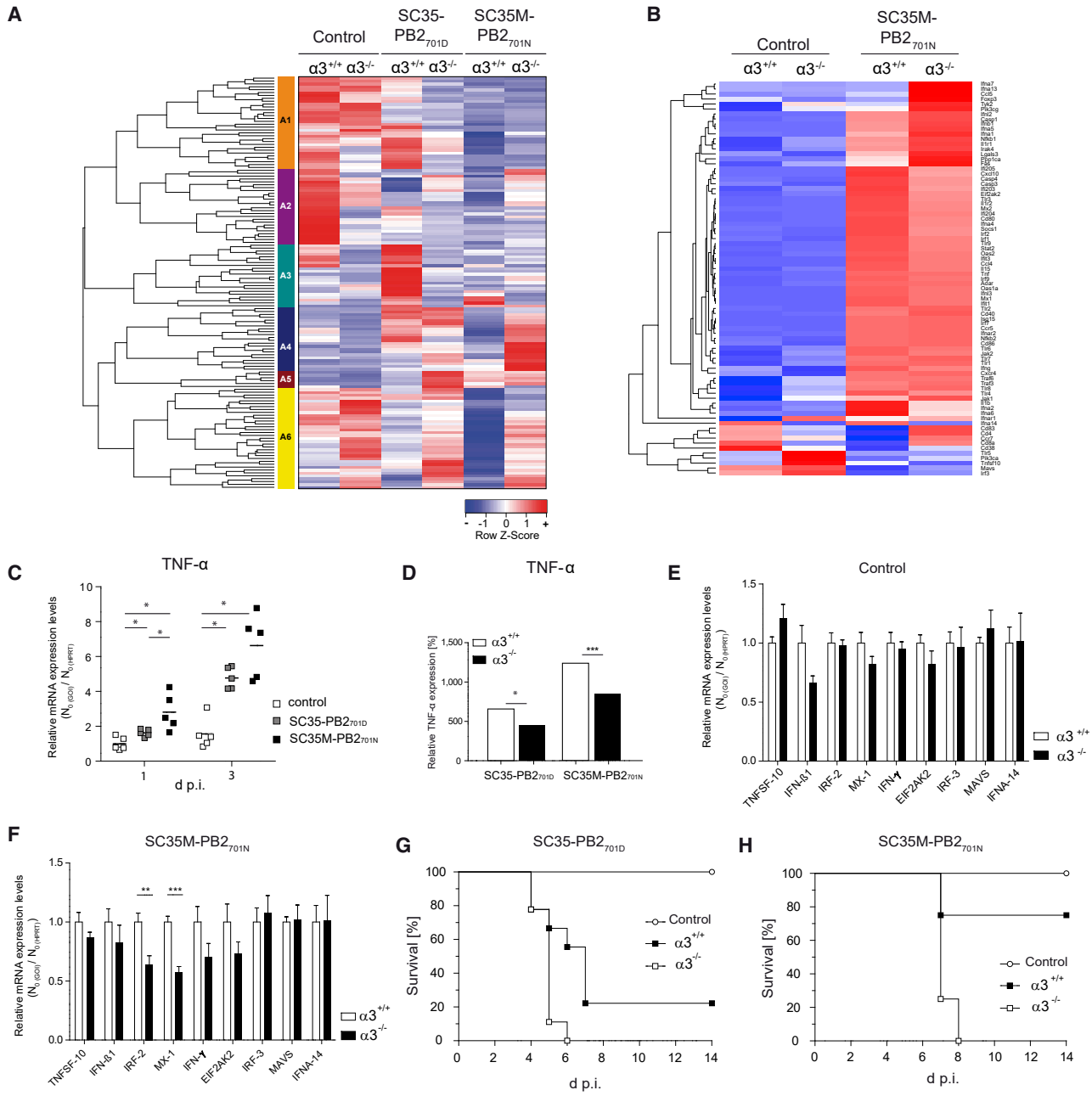

Figure 6. Genes Responsive to HPAIV Infection in Lungs of WT and Importin-α3$^{-/-}$ Mice

WT and importin-α3$^{-/-}$ (α3$^{-/-}$) mice were infected with SC35-PB2$_{701D}$ (H7N7) or SC35M-PB2$_{701N}$ (H7N7). Control mice received PBS.

(A) Heatmap depicting the row *Z* scores of the normalized expression values of 143 differentially expressed genes (p value $\leq$ 0.01 and $|\log_2 FC| \geq 1.5$) that were clustered according to their expression profiles in lungs on day 3 p.i.

(B) Heatmap depicting row *Z* scores of the normalized expression values of 79 genes with a previously described role in innate immunity (Engels et al., 2017).

(C) TNF-α expression levels detected by transcriptome analysis on day 3 p.i. in lungs of infected α3$^{+/+}$ mice relative to the maximum expression observed. Control was set to 100%.

(D) TNF-α protein levels measured by ELISA on day 1 p.i. in α3$^{+/+}$ and α3$^{-/-}$ mice. Data show average results obtained from pooled lung samples of three WT mice per virus strain (*p < 0.05; ***p < 0.001).

(E and F) Relative mRNA-expression levels of antiviral genes under an NF-κB promoter determined by qRT-PCR 3 days p.i. in control (E) and infected lungs (F) of α3$^{+/+}$ and α3$^{-/-}$ mice. Relative expression values of α3$^{+/+}$ for each gene normalized to HPRT were set to 1. Data shown represent mean ± SD (n = 5; **p < 0.01; ***p < 0.001).

(G and H) Survival in α3$^{+/+}$ and α3$^{-/-}$ mice infected with avian- (G) or human-type (H) H7N7 HPAIV. Data shown represent means ± SD (n = 9 for SC35 and n = 4 for SC53M).

HPAIV in WT as well as in $\alpha3^{-/-}$ mice revealed a subset of substantially altered expression patterns in genes involved in innate immunity (Engels et al., 2017) (Figure 6A; Tables S2 and S3). Herein, genes controlled by an NF-κB promoter were particularly prominent, with 34% of all analyzed genes (27 out of 79 hits) (Figure 6B). Moreover, literature analysis of the hits highlighted that especially genes involved in TNF pathways were of high abundance, supporting the *in vitro* findings (data not shown). TNF-α mRNA levels were increased in the lungs of human-type HPAIV-infected $\alpha3^{+/+}$ mice when compared to lungs of avian-type HPAIV-infected animals (Figure 6C). As expected, TNF-α protein expression, which is also regulated by NF-κB, was reduced in $\alpha3^{-/-}$ mice infected with both avian- and human-type HPAIV (Figure 6D). We then assessed a subset of antiviral genes under an NF-κB promoter that showed reduced expression in $\alpha3^{-/-}$ mice, such as *TNFSF-10*, *IFN-β1*, *IRF-2*, *MX-1*, *IFN-γ*, *EIF2AK2* (alias *PKR*), *IRF-3*, *MAVS*, and *IFNA-14*. While none of these genes showed significant alterations in PBS-treated control mice irrespective of the presence or absence of the importin-α3 gene (Figure 6E), the transcription, most prominently of *IRF-2* and *MX-1* genes involved in major antiviral pathways, was most significantly reduced in SC35M-$PB2_{701N}$ HPAIV-infected $\alpha3^{-/-}$ mice compared to $\alpha3^{+/+}$ mice (Figure 6F). Infection of $\alpha3^{-/-}$ mice with both SC35-$PB2_{701D}$ and SC35M-$PB2_{701N}$ resulted in enhanced weight loss and lethality compared to $\alpha3^{+/+}$ mice (Figures 6G, 6H, and S5). Virulence was significantly increased in human-type HPAIV-infected $\alpha3^{-/-}$ mice (Table S4). These data show that importin-α3 is required for the efficient expression of antiviral genes under the control of an NF-κB promoter. Failure to induce these antiviral pathways leads to high HPAIV virulence in mice.

DISCUSSION

Importin-α proteins serve as key proteins that regulate nucleocytoplamic cargo protein transport to maintain cellular homeostasis. Disruption of balanced transport pathways, caused under stress or inflammatory conditions, can cause serious diseases. In immortalized cancer cell lines, importin-α1 expression levels are particularly high compared to non-cancerous cells, as shown here as well as in many other studies before. Here, we shed light on the anatomic distribution of importin-α isoforms in the mammalian lung. We provide evidence of the highly abundant expression of importin-α3 in the murine and human RT. Moreover, importin-α isoforms are expressed as a gradient, with increasing concentrations from the URT to the LRT. Abundant and exclusive high-level expression of importin-α3 was a hallmark of the lung, unlike in other solid organs assessed, such as the liver, spleen, and brain. Knowledge on the importin-α expression pattern in the lung is important to understand the molecular basis of cellular homeostasis that might be dominated by importin-α3-transported transcription factors.

According to the crystal structure of importin-α3, which was recently solved, it was postulated that it is highly selective of cargo proteins, unlike other importin-α isoforms (Pumroy et al., 2015). The high substrate specificity is reflected by only a few cargo proteins reported to be transported into the nucleus by importin-α3. Importin-α3 seems to exclusively serve as a transporter of p53, a transcription factor involved in many cancer pathways (Marchenko et al., 2010). Importin-α3 is also a key factor in the transport of the NF-κB subunits p50 and p65 into the nucleus along with importin-α4, which is the closest relative of importin-α3 (Fagerlund et al., 2005). Mutations in ARM3 of the importin-α3 protein were shown to be crucial for p50 binding, while mutations in ARM 7 and 8 were shown to be required for p65 binding (Fagerlund et al., 2005). Based on the crystal structure of importin-α3, it was further postulated that it might pose a "fast track" nuclear import pathway under certain circumstances, such as environmental stress (e.g., viral infections), where cellular amounts of importin-β1 may be limited, requiring fast counteraction (Pumroy et al., 2015). This hypothesis is in line with our findings in this study suggesting that importin-α3 serves as a defense mechanism against influenza by promoting the nuclear entry of NF-κB, which controls the transcription of many antiviral genes.

We further show that importin-α3 gene expression is highly dynamic under inflammatory conditions. We identified an NF-κB binding site within the importin-α3 promoter element and show that its transcription is dependent on TNF-α-activated NF-κB in a concentration-dependent manner. HPAIVs that induce low-level TNF-α expression, such as those with avian-type polymerase signatures (PB2 627E and 701D), increase importin-α3 mRNA expression presumably by NF-κB induction. In contrast, high-level TNF-α expression inducing HPAIV, such as those harboring human-type polymerase signatures (PB2 627K and 701N), significantly reduces importin-α3 mRNA expression levels by a yet-unknown mechanism. One possibility would be that high numbers of NF-κB proteins may block the promoter of the importin-α3 gene and thereby its transcription. Other possible interferences could be with NF-κB-activating complexes, such as NEMO or its repressor, IκBα. Future studies are required to unravel the detailed mechanism underlying the failure of importin-α3 promoter activation. Such diverse feedback loops are known in cellular processes, where gene transcription depends on demand. Herein, generating a bottleneck in importin-α3 availability leads to failure in inducing an adequate antiviral immune response, as shown in mice lacking the importin-α3 gene. Interestingly, more than 30% of the differentially expressed genes between $\alpha3^{-/-}$ mice and their $\alpha3^{+/+}$ litter mates were under the control of an NF-κB promoter, highlighting the significant contribution of importin-α3 in NF-κB-mediated gene transcription. We could further show, using HPAIV strains of the H5N1 and H7N7 subtypes that have caused pneumonia and death in humans, that downregulation of importin-α3 mRNA transcription was a hallmark that was mediated by their human-type polymerase signatures. The introduction of avian-type polymerase signatures into the genetic backbone of these HPAIV outbreak strains restored importin-α3 mRNA transcription in the lung. It is important to note that these human-type HPAIVs induce a general cytokine storm, including TNF-α. Thus, more detailed studies are required to understand the impact of other cytokines on the transcription level of importin-α3. However, a pulmonary increase in TNF-α levels with a concomitant increase in virulence has been described for many human H5N1 and H7N7 isolates containing human-type ($PB2_{627K}$) signatures (Abdel-Ghafar et al., 2008; de Jong et al.,

2006; Hatta et al., 2001; Peiris et al., 2007; Szretter et al., 2007). Based on these findings, we propose that human-type HPAIVs have evolved mechanisms within the mammalian host to evade antiviral response pathways by high-level induction of TNF-α-activated NF-κB, which blocks the transcription of importin-α3, the major classical nuclear import protein expressed in the mammalian lung.

We have shown previously that influenza A viruses utilize differential importin-α isoforms to ensure replicative fitness (Gabriel et al., 2011). Upon zoonotic transmission of HPAIV from birds to humans, they switch from importin-α3 to importin-α7 usage. While importin-α3 acts as an inhibitor of influenza virus polymerase, importin-α7 acts as a positive factor of influenza virus replication. Importin-α7 is believed to act in a transport-independent function by a yet-unknown mechanism. Until now, it was unclear how importin-α3 mediates antiviral activity. To unravel the mechanism underlying the importin-α3-mediated inhibition, the generation of cell culture models as well as of a murine model with a deleted importin-α3 gene was essential. Our previous observation that replication of HPAIVs with avian-type polymerases, unlike HPAIV with human-type polymerases, was restricted in cells silenced using importin-α3 siRNA and is likely due to residual importin-α3 expression sufficient to induce nuclear import of NF-κB and thus the transcription of various antiviral genes. Furthermore, our findings here support the concept that avian influenza viruses evade importin-α3 restriction by blocking its transcription. As a consequence, influenza viruses get access to the second-most abundant isoform in the lung, importin-α7, to ensure high-replicative fitness in the human lung (Gabriel et al., 2011).

Finally, we here provide key insights on the dynamic role of the respiratory importin-α3 protein as an "immune sensor" of viral infections in the lung. Attempts to restore depleted importin-α3 levels in the lung might pose new strategies to treat severe respiratory virus infections.

STAR★METHODS

Detailed methods are provided in the online version of this paper and include the following:

SUPPLEMENTAL INFORMATION

Supplemental Information can be found online at https://doi.org/10.1016/j.celrep.2020.107549.

ACKNOWLEDGMENTS

The Heinrich Pette Institute, Leibniz Institute for Experimental Virology is supported by the Free and Hanseatic City of Hamburg and the Federal Ministry of Health. P.R.-I. was funded by the Alexander von Humboldt Foundation (3.3SPA/1142463 STP-2). We thank Peter König (University of Lübeck, Germany) for his support with the laser microbeam microdissection. We thank Hans-Dieter Klenk and Volker Czudai-Matwich (Philipps University of Marburg, Germany) for the human H5N1 and Ron Fouchier (Erasmus Medical Center, Rotterdam, the Netherlands) for the human H7N7 isolates. We thank Adam Grundhoff and Daniela Indenbrinken for the transcriptome analysis. We are grateful to Iris Alpers, Gökhan Arman-Kalcek, Christopher Bergfeld, Kathy Budler, Ilara Hudjetz, Lonneke Leijten, Hanna Markowsky, Annette Preuß, and Nele Twisselmann for excellent technical assistance.

AUTHOR CONTRIBUTIONS

G.G. conceived the study. G.G., S.T., and S.S.-B. designed the experiments and analyzed the data. S.T. performed all animal experiments, analyzed lung biopsy material, and performed virus replication kinetics. S.B. performed immunofluorescence assays. N.M.K. and B.T. performed qRT-PCR assays and experiments in NEMO knockout MEFs. W.B. provided NEMO knockout MEFs and discussed the data. M.Z., S.B., S.T., and S.S.-B. performed promoter activation assays. M.M. analyzed virus replication in H1299 cells. M.A., A.G., and P.R.-I. analyzed transcriptomic data. D.v.R. performed histochemical analysis of animal and human biopsies. A.O. designed studies using human biopsies and discussed the data. T.G. and S.B. performed promoter analysis studies. F.R., S.H., M.B., and E.H. generated the importin-α3 knockout mice and the respective MEFs. S.R. and A.M. performed importin sequence analysis and generated heatmaps. G.G. and S.T. wrote the manuscript.

DECLARATION OF INTERESTS

The authors declare no conflicts of interest.

Received: September 9, 2019
Revised: February 4, 2020
Accepted: March 31, 2020
Published: April 21, 2020

REFERENCES

Abdel-Ghafar, A.N., Chotpitayasunondh, T., Gao, Z., Hayden, F.G., Nguyen, D.H., de Jong, M.D., Naghdaliyev, A., Peiris, J.S., Shindo, N., Soeroso, S., and Uyeki, T.M.; Writing Committee of the Second World Health Organization

Consultation on Clinical Aspects of Human Infection with Avian Influenza A (H5N1) Virus (2008). Update on avian influenza A (H5N1) virus infection in humans. N. Engl. J. Med. *358*, 261–273.

Anders, S., and Huber, W. (2010). Differential expression analysis for sequence count data. Genome Biol. *11*, R106.

Basler, C.F., and Amarasinghe, G.K. (2009). Evasion of interferon responses by Ebola and Marburg viruses. J. Interferon Cytokine Res. *29*, 511–520.

Canton, J., Fehr, A.R., Fernandez-Delgado, R., Gutierrez-Alvarez, F.J., Sanchez-Aparicio, M.T., García-Sastre, A., Perlman, S., Enjuanes, L., and Sola, I. (2018). MERS-CoV 4b protein interferes with the NF-κB-dependent innate immune response during infection. PLoS Pathog. *14*, e1006838.

Christiansen, A., and Dyrskjøt, L. (2013). The functional role of the novel biomarker karyopherin α 2 (KPNA2) in cancer. Cancer Lett. *331*, 18–23.

Czudai-Matwich, V., Otte, A., Matrosovich, M., Gabriel, G., and Klenk, H.D. (2014). PB2 mutations D701N and S714R promote adaptation of an influenza H5N1 virus to a mammalian host. J. Virol. *88*, 8735–8742.

Dahl, E., Kristiansen, G., Gottlob, K., Klaman, I., Ebner, E., Hinzmann, B., Hermann, K., Pilarsky, C., Dürst, M., Klinkhammer-Schalke, M., et al. (2006). Molecular profiling of laser-microdissected matched tumor and normal breast tissue identifies karyopherin α2 as a potential novel prognostic marker in breast cancer. Clin. Cancer Res. *12*, 3950–3960.

de Jong, M.D., Simmons, C.P., Thanh, T.T., Hien, V.M., Smith, G.J., Chau, T.N., Hoang, D.M., Chau, N.V., Khanh, T.H., Dong, V.C., et al. (2006). Fatal outcome of human influenza A (H5N1) is associated with high viral load and hypercytokinemia. Nat. Med. *12*, 1203–1207.

Edgar, R.C. (2004). MUSCLE: multiple sequence alignment with high accuracy and high throughput. Nucleic Acids Res. *32*, 1792–1797.

Engels, G., Hierweger, A.M., Hoffmann, J., Thieme, R., Thiele, S., Bertram, S., Dreier, C., Resa-Infante, P., Jacobsen, H., Thiele, K., et al. (2017). Pregnancy-Related Immune Adaptation Promotes the Emergence of Highly Virulent H1N1 Influenza Virus Strains in Allogenically Pregnant Mice. Cell Host Microbe *21*, 321–333.

Fagerlund, R., Kinnunen, L., Köhler, M., Julkunen, I., and Melén, K. (2005). NF-κB is transported into the nucleus by importin α3 and importin α4. J. Biol. Chem. *280*, 15942–15951.

Fouchier, R.A., Schneeberger, P.M., Rozendaal, F.W., Broekman, J.M., Kemink, S.A., Munster, V., Kuiken, T., Rimmelzwaan, G.F., Schutten, M., Van Doornum, G.J., et al. (2004). Avian influenza A virus (H7N7) associated with human conjunctivitis and a fatal case of acute respiratory distress syndrome. Proc. Natl. Acad. Sci. USA *101*, 1356–1361.

Fraser, J.E., Rawlinson, S.M., Wang, C., Jans, D.A., and Wagstaff, K.M. (2014). Investigating dengue virus nonstructural protein 5 (NS5) nuclear import. Methods Mol. Biol. *1138*, 301–328.

Friedrich, B., Quensel, C., Sommer, T., Hartmann, E., and Köhler, M. (2006). Nuclear localization signal and protein context both mediate importin alpha specificity of nuclear import substrates. Mol. Cell. Biol. *26*, 8697–8709.

Frieman, M., Yount, B., Heise, M., Kopecky-Bromberg, S.A., Palese, P., and Baric, R.S. (2007). Severe acute respiratory syndrome coronavirus ORF6 antagonizes STAT1 function by sequestering nuclear import factors on the rough endoplasmic reticulum/Golgi membrane. J. Virol. *81*, 9812–9824.

Furuta, M., Kose, S., Koike, M., Shimi, T., Hiraoka, Y., Yoneda, Y., Haraguchi, T., and Imamoto, N. (2004). Heat-shock induced nuclear retention and recycling inhibition of importin alpha. Genes Cells *9*, 429–441.

Gabriel, G., Dauber, B., Wolff, T., Planz, O., Klenk, H.D., and Stech, J. (2005). The viral polymerase mediates adaptation of an avian influenza virus to a mammalian host. Proc. Natl. Acad. Sci. USA *102*, 18590–18595.

Gabriel, G., Herwig, A., and Klenk, H.D. (2008). Interaction of polymerase subunit PB2 and NP with importin alpha1 is a determinant of host range of influenza A virus. PLoS Pathog. *4*, e11.

Gabriel, G., Klingel, K., Planz, O., Bier, K., Herwig, A., Sauter, M., and Klenk, H.D. (2009). Spread of infection and lymphocyte depletion in mice depends on polymerase of influenza virus. Am. J. Pathol. *175*, 1178–1186.

Gabriel, G., Klingel, K., Otte, A., Thiele, S., Hudjetz, B., Arman-Kalcek, G., Sauter, M., Shmidt, T., Rother, F., Baumgarte, S., et al. (2011). Differential use of importin-α isoforms governs cell tropism and host adaptation of influenza virus. Nat. Commun. *2*, 156.

Goldfarb, D.S., Corbett, A.H., Mason, D.A., Harreman, M.T., and Adam, S.A. (2004). Importin α: a multipurpose nuclear-transport receptor. Trends Cell Biol. *14*, 505–514.

Görlich, D., and Mattaj, I.W. (1996). Nucleocytoplasmic transport. Science *271*, 1513–1518.

Hatta, M., Gao, P., Halfmann, P., and Kawaoka, Y. (2001). Molecular basis for high virulence of Hong Kong H5N1 influenza A viruses. Science *293*, 1840–1842.

Hu, T., Guan, T., and Gerace, L. (1996). Molecular and functional characterization of the p62 complex, an assembly of nuclear pore complex glycoproteins. J. Cell Biol. *134*, 589–601.

Huang, W., Sherman, B.T., and Lempicki, R.A. (2009). Systematic and integrative analysis of large gene lists using DAVID bioinformatics resources. Nat. Protoc. *4*, 44–57.

Hudjetz, B., and Gabriel, G. (2012). Human-like PB2 627K influenza virus polymerase activity is regulated by importin-α1 and -α7. PLoS Pathog. *8*, e1002488.

Imamoto, N., Shimamoto, T., Takao, T., Tachibana, T., Kose, S., Matsubae, M., Sekimoto, T., Shimonishi, Y., and Yoneda, Y. (1995). In vivo evidence for involvement of a 58 kDa component of nuclear pore-targeting complex in nuclear protein import. EMBO J. *14*, 3617–3626.

Kau, T.R., Way, J.C., and Silver, P.A. (2004). Nuclear transport and cancer: from mechanism to intervention. Nat. Rev. Cancer *4*, 106–117.

Kodiha, M., Chu, A., Matusiewicz, N., and Stochaj, U. (2004). Multiple mechanisms promote the inhibition of classical nuclear import upon exposure to severe oxidative stress. Cell Death Differ. *11*, 862–874.

Köhler, M., Ansieau, S., Prehn, S., Leutz, A., Haller, H., and Hartmann, E. (1997). Cloning of two novel human importin-α subunits and analysis of the expression pattern of the importin-α protein family. FEBS Lett. *417*, 104–108.

Köhler, M., Speck, C., Christiansen, M., Bischoff, F.R., Prehn, S., Haller, H., Görlich, D., and Hartmann, E. (1999). Evidence for distinct substrate specificities of importin alpha family members in nuclear protein import. Mol. Cell. Biol. *19*, 7782–7791.

Köhler, M., Fiebeler, A., Hartwig, M., Thiel, S., Prehn, S., Kettritz, R., Luft, F.C., and Hartmann, E. (2002). Differential expression of classical nuclear transport factors during cellular proliferation and differentiation. Cell. Physiol. Biochem. *12*, 335–344.

Kopecky-Bromberg, S.A., Martínez-Sobrido, L., Frieman, M., Baric, R.A., and Palese, P. (2007). Severe acute respiratory syndrome coronavirus open reading frame (ORF) 3b, ORF 6, and nucleocapsid proteins function as interferon antagonists. J. Virol. *81*, 548–557.

Kutay, U., Bischoff, F.R., Kostka, S., Kraft, R., and Görlich, D. (1997). Export of importin alpha from the nucleus is mediated by a specific nuclear transport factor. Cell *90*, 1061–1071.

Langmead, B., and Salzberg, S.L. (2012). Fast gapped-read alignment with Bowtie 2. Nat. Methods *9*, 357–359.

Lee, S.J., Matsuura, Y., Liu, S.M., and Stewart, M. (2005). Structural basis for nuclear import complex dissociation by RanGTP. Nature *435*, 693–696.

Makris, C., Godfrey, V.L., Krähn-Senftleben, G., Takahashi, T., Roberts, J.L., Schwarz, T., Feng, L., Johnson, R.S., and Karin, M. (2000). Female mice heterozygous for IKK gamma/NEMO deficiencies develop a dermatopathy similar to the human X-linked disorder incontinentia pigmenti. Mol. Cell *5*, 969–979.

Marchenko, N.D., Hanel, W., Li, D., Becker, K., Reich, N., and Moll, U.M. (2010). Stress-mediated nuclear stabilization of p53 is regulated by ubiquitination and importin-alpha3 binding. Cell Death Differ. *17*, 255–267.

Matsuura, Y., and Stewart, M. (2005). Nup50/Npap60 function in nuclear protein import complex disassembly and importin recycling. EMBO J. *24*, 3681–3689.

Neufeldt, C.J., Joyce, M.A., Levin, A., Steenbergen, R.H., Pang, D., Shields, J., Tyrrell, D.L., and Wozniak, R.W. (2013). Hepatitis C virus-induced cytoplasmic organelles use the nuclear transport machinery to establish an environment conducive to virus replication. PLoS Pathog. *9*, e1003744.

Peiris, J.S., de Jong, M.D., and Guan, Y. (2007). Avian influenza virus (H5N1): a threat to human health. Clin. Microbiol. Rev. *20*, 243–267.

Pryor, M.J., Rawlinson, S.M., Butcher, R.E., Barton, C.L., Waterhouse, T.A., Vasudevan, S.G., Bardin, P.G., Wright, P.J., Jans, D.A., and Davidson, A.D. (2007). Nuclear localization of dengue virus nonstructural protein 5 through its importin alpha/beta-recognized nuclear localization sequences is integral to viral infection. Traffic *8*, 795–807.

Pumroy, R.A., Ke, S., Hart, D.J., Zachariae, U., and Cingolani, G. (2015). Molecular determinants for nuclear import of influenza A PB2 by importin α isoforms 3 and 7. Structure *23*, 374–384.

Puthavathana, P., Auewarakul, P., Charoenying, P.C., Sangsiriwut, K., Pooruk, P., Boonnak, K., Khanyok, R., Thawachsupa, P., Kijphati, R., and Sawanpanyalert, P. (2005). Molecular characterization of the complete genome of human influenza H5N1 virus isolates from Thailand. J. Gen. Virol. *86*, 423–433.

Radu, A., Moore, M.S., and Blobel, G. (1995). The peptide repeat domain of nucleoporin Nup98 functions as a docking site in transport across the nuclear pore complex. Cell *81*, 215–222.

Ramakers, C., Ruijter, J.M., Deprez, R.H., and Moorman, A.F. (2003). Assumption-free analysis of quantitative real-time polymerase chain reaction (PCR) data. Neurosci. Lett. *339*, 62–66.

Raskatov, J.A., Meier, J.L., Puckett, J.W., Yang, F., Ramakrishnan, P., and Dervan, P.B. (2012). Modulation of NF-κB-dependent gene transcription using programmable DNA minor groove binders. Proc. Natl. Acad. Sci. USA *109*, 1023–1028.

Rexach, M., and Blobel, G. (1995). Protein import into nuclei: association and dissociation reactions involving transport substrate, transport factors, and nucleoporins. Cell *83*, 683–692.

Ruijter, J.M., Ramakers, C., Hoogaars, W.M., Karlen, Y., Bakker, O., van den Hoff, M.J., and Moorman, A.F. (2009). Amplification efficiency: linking baseline and bias in the analysis of quantitative PCR data. Nucleic Acids Res. *37*, e45.

Sankhala, R.S., Lokareddy, R.K., Begum, S., Pumroy, R.A., Gillilan, R.E., and Cingolani, G. (2017). Three-dimensional context rather than NLS amino acid sequence determines importin α subtype specificity for RCC1. Nat. Commun. *8*, 979.

Shannon, P., Markiel, A., Ozier, O., Baliga, N.S., Wang, J.T., Ramage, D., Amin, N., Schwikowski, B., and Ideker, T. (2003). Cytoscape: a software environment for integrated models of biomolecular interaction networks. Genome Res. *13*, 2498–2504.

Sievers, F., Wilm, A., Dineen, D., Gibson, T.J., Karplus, K., Li, W., Lopez, R., McWilliam, H., Remmert, M., Söding, J., et al. (2011). Fast, scalable generation of high-quality protein multiple sequence alignments using Clustal Omega. Mol. Syst. Biol. *7*, 539.

Szretter, K.J., Gangappa, S., Lu, X., Smith, C., Shieh, W.J., Zaki, S.R., Sambhara, S., Tumpey, T.M., and Katz, J.M. (2007). Role of host cytokine responses in the pathogenesis of avian H5N1 influenza viruses in mice. J. Virol. *81*, 2736–2744.

Todaro, G.J., and Green, H. (1963). Quantitative studies of the growth of mouse embryo cells in culture and their development into established lines. J. Cell Biol. *17*, 299–313.

Walther, T., Balschun, D., Voigt, J.P., Fink, H., Zuschratter, W., Birchmeier, C., Ganten, D., and Bader, M. (1998). Sustained long term potentiation and anxiety in mice lacking the Mas protooncogene. J. Biol. Chem. *273*, 11867–11873.

Wang, P., Palese, P., and O'Neill, R.E. (1997). The NPI-1/NPI-3 (karyopherin alpha) binding site on the influenza a virus nucleoprotein NP is a nonconventional nuclear localization signal. J. Virol. *71*, 1850–1856.

Yasuda, Y., Miyamoto, Y., Yamashiro, T., Asally, M., Masui, A., Wong, C., Loveland, K.L., and Yoneda, Y. (2012). Nuclear retention of importin α coordinates cell fate through changes in gene expression. EMBO J. *31*, 83–94.

Yasuhara, N., Shibazaki, N., Tanaka, S., Nagai, M., Kamikawa, Y., Oe, S., Asally, M., Kamachi, Y., Kondoh, H., and Yoneda, Y. (2007). Triggering neural differentiation of ES cells by subtype switching of importin-alpha. Nat. Cell Biol. *9*, 72–79.

STAR★METHODS

KEY RESOURCES TABLE

REAGENT or RESOURCE	SOURCE	IDENTIFIER
Antibodies		
importin-α1	Abcam	ab6036; RRID: AB_305245, ab54489; RRID: AB_2249727
importin-α3	Abcam	ab6039; RRID: AB_1977565
importin-α3	Novus Biologicals	#NB100-93345; RRID: AB_1237130, replaced by #NB100-81651; RRID: AB_1146049
importin-α4	Abcam	ab6038; RRID: AB_305247
importin-α5/7	University of Lübeck	Köhler et al., 1999
NF-κB p65	Cell Signaling	#3987; RRID: AB_2341215
Virus Strains		
SC35-PB2$_{701D}$	University of Marburg	Gabriel et al., 2011
SC35M-PB2$_{701N}$	University of Marburg	Gabriel et al., 2011
A/Thailand/1(KAN-1)/2004 (H5N1)	University of Marburg	Puthavathana et al., 2005
A/Netherlands/219/2003	Erasmus Medical Center	Fouchier et al., 2004
Biological Samples		
Human biopsy material from nasal concha and the lung	Erasmus Medical Center Rotterdam, the Netherlands	#MEC-2011-129, MEC 2008-207, MEC 2009-128
Chemicals, Peptides and Recombinant Proteins		
Human TNF-α	R&D Systems	#210-TA
Mouse TNF-α	BioLegends	#575204
Critical Commercial Assays		
Dual-Luciferase ® Reporter Assay System	Promega	E1910
LightSwitch Luciferase Assay Reagent	SwitchGear Genomics	LS010
Deposited Data		
European Nucleotide Archive (ENA)	Heinrich Pette Institute, Hamburg	https://www.ebi.ac.uk/ena/data/view/PRJEB8023
Experimental Models: Cell Lines		
Importin-α3$^{-/-}$ MEFs	Max Delbrück Center, Berlin	This study
Importin-α3$^{-/-}$ H1299	Heinrich Pette Institute, Hamburg	This study
NEMO$^{-/-}$ MEFs	Heinrich Pette Institute, Hamburg	Makris et al., 2000
HBEpC	PromoCell	C-12640
HSAEpC	PromoCell	C-12642
Experimental Models: Organisms/Strains		
Importin-α3$^{-/-}$ mice	Max Delbrück Center, Berlin	This study
Recombinant DNA		
pLightSwitch_Prom-importin-α3	SwitchGear Genomics	This study
pLightSwitch_Prom-control	SwitchGear Genomics	This study
Software and Algorithms		
Muscle version 3.8.1551	Not applicable	Edgar, 2004
Clustal Omega version 1.2.4	Not applicable	Sievers et al., 2011

LEAD CONTACT AND MATERIALS AVAILABILITY

Further information and requests for resources and reagents should be directed to and will be fulfilled by the Lead Contact, Guelsah Gabriel (guelsah.gabriel@leibniz-hpi.de). Materials, reagents and mouse lines of this study are available with a completed Material Transfer Agreement.

EXPERIMENTAL MODEL AND SUBJECT DETAILS

Human Subjects

Biopsy material from human uninfected URT (nasal concha) and LRT (lung, mainly consisting of alveolar tissue) was obtained from the Erasmus Medical Center in Rotterdam, the Netherlands, from donors at the Erasmus Medical Center in Rotterdam. Approval to use the clinical samples for scientific use was obtained from the Dutch Medical Ethical Committee under the permit numbers #MEC-2011-129, MEC 2008-207 and MEC 2009-128. Donor sex and age is unknown.

Cells and Viruses

Cell lines of human embryonic kidney cells (HEK293T, ATCC), human alveolar adenocarcinoma cells (A549, H1299, ATCC), african green monkey kidney cells (VeroE6) and human cervical adenocarcinoma cells (HeLa, ATCC) were grown in Dulbecco's modified Eagle's medium (DMEM, PAA) supplemented with 10% fetal calf serum (FCS; PAA), 1% penicillin/streptomycin (P/S, PAA), and 1% L-Glutamine (PAA). Mouse embryonic fibroblasts (MEF, see description of their generation in a separate paragraph below) were grown in DMEM supplemented with 10% FCS, 1% P/S, 1% L-Glutamine, 1% sodium pyruvate, and 1% non-essential amino acids (NEAA, PAA). Immortalized NEMO$^{-/-}$ MEFs (Makris et al., 2000) were kindly provided by Michael Karin (University of California, San Diego). Madin Darby canine kidney cells (MDCKII, ATCC) were grown in Minimal Essential Medium (MEM, PAA) supplemented with 10% FCS, 1% P/S, and 1% L-Glutamine. Primary human bronchial (HBEpC, PromoCell, C-12640) and primary human small airway epithelial cells (HSAEpC, PromoCell, C-12642) were grown in Airway Epithelial Cell Media or Small Airway Epithelial Cell Media (PromoCell), respectively, supplemented with 1% P/S. HBEpC cell donor was a 52 year old female subject. HSAEpC cell donor was a 57 year old female subject. Cells were cultivated at 5% CO_2, 96% rH and 37°C. Recombinant H7N7 HPAIV viruses SC35-PB2$_{701D}$, SC35M-PB2$_{701N}$, the single-point mutants SC35-PB2$_{701N}$ and SC35-NP$_{319K}$ or the double mutant SC35-PB2$_{701N}$-NP$_{319K}$ (Gabriel et al., 2011) as well as recombinant A/Thailand/1(KAN-1)/2004 (H5N1) wild-type strain (H5N1-PB2$_{701N}$) (Gabriel et al., 2011; Puthavathana et al., 2005), the avian-type single point mutant thereof (H5N1-PB2$_{701D}$) and H7N7 HPAIV virus isolates A/Netherlands/219/2003 (H7N7-PB2$_{627K}$, fatal case) or the recombinant virus thereof (H7N7-PB2$_{627E}$) (Czudai-Matwich et al., 2014; Fouchier et al., 2004) were used.

All experiments with H5N1 and H7N7 viruses were conducted at the Heinrich Pette Institute, Leibniz Institute for Experimental Virology in Hamburg, Germany, in biosafety level 3 facilities, except for the SC35M-PB2$_{701N}$ strain that was classified as biosafety level 2 agent, and approved by the relevant German authorities (Gentechnikbehörde Hamburg).

Animals

Importin-α3$^{-/-}$ mice in the C57BL/6 genetic background and WT littermates thereof were bred and housed under specific pathogen-free conditions at the animal facility of the Heinrich Pette Institute, Leibniz Institute for Experimental Virology, Hamburg, Germany. We used 6-12 week old female and male mice. Experimental groups were matched regarding equal numbers of female and male mice as well matched in comparable age groups.

Animal experiments were performed in strict accordance with the guidelines of the German Animal Welfare Regulations. All animal protocols were approved by the relevant German authority (Behörde für Stadtentwicklung und Umwelt Hamburg, license numbers: 29/09, 54/11). Mice were humanely killed upon > 25% weight loss or upon achievement of defined body index scores (e.g., on physical appearance, clinical signs, behavior, eating and drinking etc.) according to the German Animal Welfare Regulations.

METHOD DETAILS

Transfection and Vectors

Transfections were performed using Lipofectamine 2000 (Invitrogen) or jetPRIME® (Polyplus-Transfection) according to the manufacturer's instructions. Vector constructs used were pHW2000-(SC35-PB2$_{701D}$, SC35-PB2$_{627K}$, SC35-PB1, SC35-PA, SC35-NP, SC35M-PB2$_{701N}$, SC35M-PB1, SC35M-PA, SC35M-NP) (Gabriel et al., 2005), pcDNA-importin-α1-N-FLAG, pcDNA-importin-α3-N-FLAG, pcDNA-importin-α5-N-FLAG and pcDNA-importin-α7-N-FLAG, pPol-I-NP-Luc-human (Gabriel et al., 2005), pRL-TK (Promega), pLightSwitch_Prom-control and pLightSwitch_Prom-importin-α3 (renilla luciferase reporter constructs; SwitchGear Genomics), pFL-TK and pCMVTAG-NEMO (Addgene). The pcDNA-importin-α-N-FLAG constructs were described previously (Gabriel et al., 2011; Wang et al., 1997). pFL-TK was generated by amplification of the firefly luciferase gene from the pPol-I-NP-luc-human construct (Gabriel et al., 2005) using primers p5_NheI_Fluc_for (5′-GCGCTAGCCACCATGGAAGACGCCAAAAACATAAAGAA AGGCCCGGC-3′) and p3_Fluc_NotI_rev (5′-GCGCGGCCGCTTACAATTTGGACTTTCCGCCCTTCTTGG-3′). Insertion of the firefly luciferase gene into pRL-TK without the renilla luciferase gene was performed via the NheI and NotI restriction sites.

Antibodies

Primary antibodies used for western blot and immunohistochemical analyses include goat anti-importin-α1 (Abcam, ab6036), rabbit anti-importin-α1 (Abcam, ab54489), goat anti-importin-α3 (Abcam, ab6039), goat anti-importin-α4 (Abcam, ab6038), rabbit anti-importin-α3 (Novus Biologicals, #NB100-93345, replaced by #NB100-81651), rabbit anti-importin-α3 (Köhler et al., 1997), rabbit anti-importin-α5/α7 (Köhler et al., 1999), rabbit anti-NF-κB p65 (Cell Signaling, #3987), rabbit anti-LSD1 (Cell Signaling, #2139), rabbit

anti-GAPDH (Cell Signaling, #2118), mouse anti-nuclear matrix protein p84 (Abcam, ab487), mouse anti-FLAG M2 (Sigma-Aldrich, #F3165), rabbit anti-HA (Sigma-Aldrich, #H908), mouse anti-influenza A virus nucleoprotein (HB65; American Type Culture Collection, Manassas, VA) antibodies and rabbit anti-FPV serum (Gabriel et al., 2008). Anti-rabbit-HRP, anti-goat-HRP, anti-mouse-HRP (Sigma-Aldrich, #A8275, #A5420, and #A4416, respectively), and IRDye-conjugated anti-rabbit (Li-Cor) antibodies were used as secondary antibodies for western blot.

Importin-α sequence analysis

Nucleotide sequences of the coding regions of importin-α1, importin-α3, importin-α4, importin-α5, importin-α6 and importin-α7 were downloaded from the NCBI nucleotide database for *Homo sapiens* (GenBank: NM_001320611.1, NM_002268.5, NM_002267.4, CR456743.1, NM_001366307.2, NM_012316.5), Macaca fascicularis (GenBank: NM_001283904.1, XM_005546256.2, XM_005585866.2, XM_005547987.2, XM_005551660.2, XM_005544119.2), Sus scrofa (GenBank: NM_001163404.1, XM_021069735.1, NM_001193575.1, NM_001163405.1, XM_005654393.3, XM_021095806.1), *Mus musculus* (GenBank: NM_010655.3, NM_008467.4, NM_008466.5, BC006771.1, NM_008468.4), Gallus gallus (GenBank: NM_001006209.1, NM_001007963.1, NM_001193575.1, NM_001030774.1, XM_015284586.2, NM_001012841.2) and Anas platyrhynchos (GenBank: XM_005012314.3, XM_027464723.1, XM_027471420.1, XM_027449713.1, XM_027454663.1). For *Mus musculus*, no importin-α6 sequence was available, while the importin-α7 sequence was missing for Anas platyrhynchos. The nucleotide sequences were subsequently translated into amino acid sequences using the standard genetic code. For each Importin-α, the sequences were aligned using Muscle version 3.8.1551 (Edgar, 2004) with standard parameters. Pairwise nucleotide and amino acid sequence identities were then calculated using Clustal Omega version 1.2.4 (Sievers et al., 2011).

Generation of Importin-α3$^{-/-}$ Mice and Importin-α$^{-/-}$-MEFs

To generate an importin-α3 targeting construct, a 900 bp-long sequence upstream and a 5100 bp-long sequence downstream of exon 1 of the importin-α3 gene were cloned into a targeting vector described before (Walther et al., 1998). After homologous recombination in embryonic stem (ES) cells, exon 1 bearing the translational start site for the importin-α3 protein, was deleted. ES cells were electroporated with the linearized construct and clones were picked after double selection with neomycin and gancyclovir. Positive clones were identified by PCR and one of them was chosen for blastocyst injection. From the injected ES cell clone, germline chimeras were obtained and bred with C57BL/6 mice. Importin-α3 deficient mice were backcrossed for eight generations to the C57BL/6 genetic background; the colony was maintained by breeding heterozygous mice. For genotyping, the following primers were used for PCR on genomic DNA of tail or ear biopsies: Impa3for 5'-CCCTCAGTGTGAATTACTTCC-3'; Impa3rev 5'-GAGTC CAAAGCCACTTCGAG-3'; Impa4neorev 5'-GCCCAGTCATAGCCGAATAG-3'. To confirm the gene deletion, absence of importin-α3 mRNA and protein was determined by RT-PCR and western blot of organs. Absence of importin-α3 mRNA with β-Actin as reference was verified using the following primers: Impa3Ex1_for 5′-GACAACGAGAAATTGGACAACC-3′; Impa3Ex7_rev 5′-CGTTCCAGATGCAATGTTTGTC-3′; beta-actin_for 5′-TACAATGAGCTGCGTGTG-3′; beta-Actin_rev 5′-CACAGCCTGGATGGC TAC-3′. Wild-type (WT) and importin-α$^{-/-}$ murine embryonic fibroblasts (MEFs) were prepared from murine embryos harvested on embryonic day 13.5 from pregnant females. To obtain immortalized cell lines, primary MEFs were passaged at least 25 times according to an adaption of the 3T3 protocol (Todaro and Green, 1963).

Generation of Importin-α3$^{-/-}$ Cell Lines

To generate H1299 importin-α3$^{-/-}$ and control importin-α3$^{+/+}$ cell lines, the cells were seeded in 12 wells and transfected using Lipofectamine 2000 (Invitrogen) with either a control CRISPR-Cas9 plasmid or an importin-α3$^{-/-}$ CRISPR-Cas9 plasmid (Santa Cruz Biotechnology). 48 hours post transfection positive cells were sorted via FACS into 96 well plates with help of a green fluorescent protein selection marker. Clones were tested via western blot for importin-α3 expression and positive clones were cultivated further for cryopreservation.

Animal Experiments

Mice were anaesthetized with ketamine-xylazine (70 mg/kg and 7 mg/kg, respectively) and intranasally infected with the respective virus dose in 50 μl 1x PBS. WT mice were infected with 6*10^4 p.f.u. (100-fold MLD_{50} of SC35M-$PB2_{701N}$ in BALB/c mice [9]) of SC35-$PB2_{701D}$, SC35M-$PB2_{701N}$, the single-point mutants SC35-$PB2_{701N}$ or SC35-NP_{319K} or the double mutant SC35-$PB2_{701N}$-NP_{319K}. Control groups received PBS. On day 3 p.i., five animals per time point were anaesthetized with an overdose of ketamine-xylazine (140 mg/kg and 14 mg/kg, respectively) and sacrificed after intracardial perfusion with DEPC-treated 1x PBS. Perfused organs (lung, trachea, liver, spleen, brain) were removed and dissected into pieces (< 5 mm) and submerged in RNA*later* RNA Stabilization Reagent (QIAGEN). Murine URT samples were obtained by decapitation of the head above the atlas. After skinning and sagittal division of the head, the tissue of the nasal concha was excised and submerged in RNA*later*.

For relative mRNA-Expression levels determination of antiviral genes under an NF-κB promoter by RT-qPCR, WT (n = *5*) and importin-α3$^{-/-}$ (n = *5*) mice were infected with 10^6 p.f.u. of SC35M. Control groups received PBS. On day 3 p.i., five animals were anaesthetized with an overdose of ketamine-xylazine and sacrifice. Whole lungs were removed and dissected into pieces and submerged

in RNA*later*. Organs (lung, spleen, brain) of uninfected WT mice (n = 3) for western blot lysate preparation were obtained after short inhalative isoflurane narcosis followed by cervical dislocation. After dissection into small pieces, the organs were immediately frozen on dry ice.

For virus titer determination of organs, WT (n = 3) and importin-$\alpha3^{-/-}$ (n = 3) mice were infected with $6*10^4$ p.f.u. of SC35-PB2$_{701D}$ (~0,1x MLD$_{50}$ of SC35-PB2$_{701D}$ in C57BL/6 mice) or a low and high dose of SC35M-PB2$_{701N}$ (10^3 p.f.u.; ~0,5x MLD$_{50}$ or $6*10^4$ p.f.u.; ~30x MLD$_{50}$ of SC35M-PB2$_{701N}$, respectively). On days 3 and 6 p.i., three animals per time point were sacrificed, organs (lung, trachea, brain) removed, virus titers determined by plaque assay [64], and the URT and LRT stained immunohistochemically against influenza virus and importin-α antigen. For this, murine formalin-fixed, paraffin-embedded (FFPE) lungs or skinned, decalcified FFPE heads were thin sectioned (3 μm). Heads were decalcified in 10% EDTA (pH 7,4) for 8 days, followed by sagittal division and incubation in same solution for 3 more days. Mouse lethal dose 50 (MLD$_{50}$) was assessed by infecting WT (n = 4-9) and importin-$\alpha3^{-/-}$ (n = 4-9) mice with serial virus dilutions of SC35-PB2$_{701D}$ (10^5, $5*10^5$, and 10^6 p.f.u.) or SC35M-PB2$_{701N}$ (10^2, 10^3, and 10^4 p.f.u.). Animals were monitored for weight and survival for 14 days p.i. and the MLD$_{50}$ was calculated. Humane endpoints were defined according to the German Animal Welfare Regulations as described above.

Immunohistochemical Analysis (IHC-P)

Viral and importin-α1, -α3, and -α7 antigen were determined by IHC-P with antigen-specific primary and HRP-conjugated secondary antibodies. URT and lungs of infected WT and importin-$\alpha3^{-/-}$ mice were excised on days 1 and 3 p.i.. FFPE thin-sections (3 μm) of murine samples and human biopsies were prepared as described (Gabriel et al., 2009). Viral antigen was stained using the mouse anti-influenza A nucleoprotein (HB65; American Type Culture Collection, Manassas, VA) or the rabbit anti-FPV-serum, a biotin-conjugated anti-rabbit secondary antibody (Jackson ImmunoResearch, #711-066-152), the *Avidin/Biotin Blocking Kit SP2001* (Biozol), and the *ZytoChemPlus (HRP) Broad Spectrum (DAB) Kit* (Zytomed) according to the manufacturer's instructions. For visualization of importin-α isoforms in murine and human FFPE samples, the described rabbit anti-importin-α1, rabbit anti-importin-α3 (Novus Biologicals), and rabbit anti-importin-α5/α7 antibodies were used together with a biotin-conjugated anti-rabbit secondary antibody (DAKO; #E0432), a peroxidase-conjugated avidin-biotin-complex-reaction kit (DAKO), and the HRP substrate AEC (DAKO). Counterstaining was performed with hematoxylin. Since the importin-α7 antibody, cross-reacts with importin-α5, lung tissues of mice with a deletion of either the importin-α5 or the -α7 gene were additionally used as controls (data not shown). To exclude false-positive staining due to cross-reactivity of the antibodies, FFPE thin sections were additionally stained using importin-α isoform-specific blocking peptides for importin-α1 (aa518-529, QVQDGAPGTFNF, GenScript), importin-α3 (aa509-521, NSSANVPTEGFQF, Abcam, #ab23144), importin-α5 (aa3-16, TPGKENFRLKSYKN, GenScript) and importin-α7 (aa3-12, MASPGKDNYR; aa526-536, PEAPMEGFQL, GenScript) in different concentrations (0.2 μg/ml, 2 μg/ml, and 20 μg/ml) (Table S5). Primary antibodies were incubated with the respective peptides for 30 min prior to IHC-P. No unspecific staining was observed with 2 μg/ml and 20 μg/ml of peptide (data not shown). Images were acquired using a NIKON AZ100 wide field light microscope with a NIKON DS-Ri1 high-resolution microscope camera, AZ Plan Fluor 5x and AZ Plan Apo 1x objectives, and the *NIKON Digital Sight DS-L2 Imaging Controller*. Image processing was performed using *Adobe® Photoshop® CS4 Extended v.11.0.2*.

Laser Microbeam Microdissection (LMM)

LMM was performed on murine lung cryosections to obtain bronchiolar epithelium and alveolar tissue samples using the *PALM MicroBeam System* (*Axiovert 200* microscope incl. *PALM CapMover*, *PALM RoboStage I*, *PALM RoboSoftware v2.2.*; P.A.L.M. Microlaser Technologies GmbH/ZEISS). After thoracotomy of WT C57BL/6 mice, lungs were filled with *Tissue Tek® Compound* (50% in 1x PBS, Sakura Finetek) and were shock-frozen in melting isopentane. Cryosections (10 μm) were generated at the *Cryostat CM3050 S* (LEICA), let dry for 5 min at −20°C and stained with cresyl violet (2 min 70% ethanol, −20°C; 2 s 1% cresyl violet in 50% ethanol, RT; 30 s 70% ethanol, −20°C; 30 s 100% ethanol).

RNA Isolation

Total RNA from cells or tissue samples was isolated using the *innuprep RNA Minikit* (Analytik Jena). Homogenization of ~50 mg of RNA*later*-fixed organs was performed in 450 μl lysis buffer RL with 10 sterile, stainless steel beads (Ø 2 mm, #22.455.0010, Retsch) at 30 Hz and 4°C for 6 min in the mixer mill MM400 (Retsch). *RNase free DNase Set* (QIAGEN) was used for on-column DNase I-treatment. After elution in RNase-free water, 1 U/μl *Ribolock RNase Inhibitor* (Thermo Scientific) was added. RNA concentration and purity were determined using the *Nanodrop 1000* (Peqlab). Microdissected murine tissue was vortexed for 1 min in lysis buffer RL, incubated for 30 min at RT and vortexed again (1 min). After short centrifugation, the lysate was stored at −80°C overnight. After thawing, 1 min of vortexing, and centrifuging (8 s), the sample was mixed ten times with 700 μl of 70% ethanol using a needle and syringe. RNA was isolated according to the *innuprep RNA Minikit*'s instructions. Total RNA from human FFPE URT was isolated from 1-2 sections (20 μM) after xylene deparaffinization using the *QIAGEN RNeasy® FFPE Kit* (QIAGEN). Isolated RNA was either processed immediately or stored at −80°C.

cDNA Generation

cDNA from tissues or cells was generated using random primers and the SuperScript III Reverse Transcriptase (Invitrogen) according to the manufacturer's instructions. Random nonamer primer (Gene Link, pd(N)9, 26-4000-06, final concentration: 5 μM) and dNTP

mix (QIAGEN, final concentration: 500 μM each dNTP) were incubated for 5 min at 65°C with 5 μg of total RNA in a final volume of 13 μl and cooled for at least 1 min on ice. Then, 1x First Strand Buffer, DTT (final concentration: 5 mM), RiboLock RNase Inhibitor (Thermo Scientific, final concentration: 2 U/μl), and 10 U/μl SuperScript III Reverse Transcriptase were added (final reaction volume: 20 μl). cDNA was generated using the GeneAmp® PCR System 9700 (Applied Biosystems; cycle: 25°C for 5 min, 50°C for 60 min, 70°C for 15 min, 4°C for ∞).

cDNA from microdissected samples was generated using the RevertAid H Minus Reverse Transcriptase (Thermo Scientific). 2 μl of total RNA were treated with 1 U/μl DNase I and 1x DNase I buffer (Sigma-Aldrich, #AMPD1) for 15 min at RT (reaction volume: 10 μl). DNA restriction was stopped by adding 1.5 μl 50 mM EDTA and incubation for 10 min at 70°C. Then, 1x Reaction Buffer, DTT (final concentration: 500 μM), dNTP-Mix (Peqlab; final concentration: 500 μM each dNTP), 250 ng random hexamer primer (pd(N)6, Eurofins MWG Operon), and 100 U RevertAid H Minus Reverse Transcriptase were added (final reaction volume: 20 μl). cDNA was generated using the cycle 42°C for 50 min, 70°C for 15 min, and 4°C for ∞.

For cDNA from human FFPE URT, 250 ng of total RNA were incubated with Random Primers (Promega, 500 μg/ml, # C1181; final concentration: 500 ng) and dNTP mix (final concentration: 500 μM each dNTP) for 5 min at 65°C in a volume of 13 μl. After cooling (at least 1 min on ice), 1x First Strand Buffer, DTT (final concentration: 5 mM), RNasin® Ribonuclease Inhibitor (Promega, #N251B; final concentration: 2 U/μl) and 10 U/μl SuperScript III Reverse Transcriptase were added (final reaction volume: 20 μl). cDNA was generated using the following cycle: 25°C for 5 min, 50°C for 45 min, 70°C for 15 min, and 4°C for ∞. All cDNA samples were processed immediately or stored at −20°C.

Design of RT-qPCR Primers

DNA oligonucleotides (Sigma-Aldrich; Table S6 for RT-qPCR were designed using Clone Manager 9 Professional Edition or Primer-BLAST (https://www.ncbi.nlm.nih.gov/tools/primer-blast/index.cgi).

Real-Time Quantitative PCR (RT-qPCR)

Gene of interest (GoI) mRNA expression levels were determined using specific primer pairs (Table S6). Singleplex reactions (10 μl) were set up manually in UltraPure DNase/RNase-Free Distilled Water (GIBCO) in MicroAmp® Optical 96-Well Reaction Plates (Invitrogen, #4306737): 5 μl Platinum® SYBR® Green qPCR SuperMix-UDG (2x, Invitrogen), 0.02 μl ROX Reference Dye (25 μM, Invitrogen, final concentration: 50 nM), 300 nM of forward and reverse primer each, and 1 μl cDNA template. RT-qPCR runs were conducted on the ABI 7500 Fast System (Applied Biosystems) in the Standard 7500 mode with endpoint fluorescence detection: 2 min at 50°C, 3 min at 95°C, 50 amplification cycles (15 s at 95°C, 10 s at 65°C, and 30 s at 72°C). Analysis was performed in triplicate or quadruplicate for each GOI and GAPDH in each sample. Subsequently, melting curve analysis was performed on the ABI 7500 Fast System (15 s at 95°C, 1 min at 60°C, 15 s at 95°C). Correct amplicon size was checked by agarose gel electrophoresis. Data of reactions with false products was excluded from data analyses. Relative expression values were determined using the $E^{-\Delta\Delta CT}$-method (Ramakers et al., 2003; Ruijter et al., 2009). The Rn-values were exported from the SDS Software v1.3.1 (Applied Biosystems) to Microsoft Office Excel 2007 and N_0-values for the starting concentration of the transcript in the original sample were obtained with LinReg PCR Software v11.1 (Ruijter et al., 2009). The averaged N_0-value of the GOI (e.g., $N_{0\ (importin\text{-}\alpha3)}$, n = 3–4 technical replicates) was then normalized with the averaged N_0-value for GAPDH ($N_{0\ (GAPDH)}$) of the respective sample. The relative $N_{0(GOI)}/N_{0\ (GAPDH)}$-expression values of the biological replicates are presented. For easier comparison of differential expression, the averaged relative N_0-value was set 1. Relative mRNA expression levels of NF-κB regulated genes were determined using specific primer pairs (Table S6) for the genes of interest (GOIs) and the reference gene HPRT. Singleplex reactions (20 μl) were set up manually in H_2O PCR grade (ROCHE®) in LightCycler® 480 Multiwell Plate 96 (ROCHE®, #04729692001): 10 μl FastStart Essential DNA Green Master (2x, ROCHE®), 300 nM of forward and reverse primer each, and 2 μl cDNA template. RT-qPCR runs were conducted on the LightCycler® 96 Real-Time PCR System (ROCHE®) with endpoint fluorescence detection: 10 min at 95°C, 50 amplification cycles (15 s at 95°C, 10 s at 65°C, and 20 s at 72°C). Analysis was performed in triplicate for each GOI and HPRT in each sample. Subsequently, melting curve analysis was performed (15 s at 95°C, 15 s at 60°C, 1 s at 95°C). Correct amplicon size was checked by agarose gel electrophoresis. The relative $N_{0(GOI)}/N_{0\ (HPRT)}$-expression values of the biological replicates are presented.

Protein Extraction and Purification

Whole cell lysates (WCL) of cells were obtained by lysis in HEPES lysis buffer (50 mM HEPES (pH 8.0), 200 mM NaCl, 0.5% IGEPAL, 25% glycerol, 1 mM PMSF, 0,07 μl/ml β-mercaptoethanol, 1x HALT Protease and Phosphatase Inhibitor Cocktail, 1x EDTA Solution) or samples were fractionated into cytoplasmic (CF) and nuclear fractions (NF) using the NE-PER Nuclear and Cytoplasmic Extraction Reagents (Thermo Fisher Scientific Inc.). Whole organ lysates of uninfected WT mice were obtained by weighing ~30 mg of tissue into O-ring tubes filled with 8 stainless steel beads (Ø 2 mm, #22.455.0010, Retsch). After washing the organ pieces once with 800 μl 1x PBS and centrifugation at 500 xg and 4°C for 5 min, the supernatant was discarded and 10 μl HEPES lysis buffer per mg organ were added. Homogenization was carried out at 4°C and 20 Hz for 2 min followed by 30 Hz for 1 min in the mixer mill MM400 (Retsch). The homogenates were then incubated for 5 min on ice and subsequently centrifuged for 20 min at 21,000 xg and 4°C. The supernatant was transferred into a fresh tube, mixed with 4x protein loading dye and boiled for 5 min at 95°C before being subjected to western blot analysis. Whole cell lysates of HEK293T cells transfected with 10 μg of each of the pcDNA-importin-α-N-FLAG constructs were subjected to affinity purification using the EZview Red ANTI-FLAG M2 affinity gel (Sigma-Aldrich) and eluted using a 3x FLAG peptide

(Sigma-Aldrich) according to the manufacturer's instructions. Thus, purified FLAG-tagged importin-α isoforms were obtained and used to generate standard curves to determine the affinities of the different isoform-specific importin-α antibodies. The protein amounts of each isoform were quantified in murine organ homogenates using western blot analyses and standardized using the individual standard curves as described previously (Köhler et al., 2002, 1999).

Western Blot

Successful knockdown of importin-α isoforms was confirmed by western blot analysis using the described goat anti-importin-α1, goat anti-importin-α3, goat anti-importin-α4, and rabbit anti-importin-α5/α7 antibodies, respectively, with normalization to GAPDH using the rabbit anti-GAPDH antibody. The same antibodies were used for detection and quantification of endogenous importin-α isoforms in cell or organ lysates. For detection and quantification of FLAG-tagged importin-α isoforms, the mouse anti-FLAG M2 antibody was used. Amounts of viral NP protein or NF-κB p65 in cell lysates after viral infection or TNF-α treatment were quantified using the rabbit anti-FPV serum and the rabbit anti-NF-κB p65 antibodies, respectively. For detection of HA-tagged NEMO, the rabbit anti-HA antibody was used. Equal amount of protein was loaded for each sample using GAPDH, p84 or LSD1 as loading control. Quantification of protein was performed with the *Bioimager Image Quant LAS 4000* at non-saturated levels with GAPDH or LSD1 adjustment for WCL, GAPDH adjustment for CF, and LSD1 of p84 adjustment for NF. Alternatively, NP levels were adjusted and used for normalization.

Immunofluorescence

WT MEFs as well as MEFs deficient for importin-α3 were seeded in glass bottom dishes (#81218-200, Ibidi GmbH) using regular growth medium (10% FBS, 1% P/S, 1% L-Glutamine, 1% NEAA, 1% sodium pyruvate). After 8h, the growth medium was replaced with starvation medium (serum reduced to 0.5% FBS) and cells were starved for another 16h. Subsequently, cells were either control-treated or treated with murine TNF (10 ng/ml; #575204, BioLegend, Inc) for 15 min at 37°C. Then, immunofluorescence staining was performed. All washing steps were performed with phosphate buffered saline (PBS), and all incubation steps were performed at room temperature, if not otherwise stated. Briefly, cells were washed and fixed with 4% paraformaldehyde (in PBS) for 10 min at 37°C. Fixed cells were washed twice and permeabilized with 0.1% Triton X-100 (in PBS) for 20 min. After washing, cells were blocked with 3% bovine serum albumin (BSA) solution (in PBS) and then incubated with a primary antibody recognizing murine NF-κB p65 subunit (1:300 in 3% BSA/PBS; #8242S, Cell Signaling) for 1h. Cells were washed again and incubated for 1h with a donkey anti-rabbit IgG antibody coupled to Alexa-555 dye (1:500 in 3% BSA/PBS; A31572, Life Technologies GmbH). This step also included staining of nuclei with Hoechst dye (1:1000 in 3% BSA/PBS; #62249, Life Technologies GmbH). After further washing, stained cells were stored in PBS at 4°C. Images were acquired on a confocal Nikon Eclipse Ti-E spinning disc microscope (Nikon, Japan) at 100-fold magnification. Image processing was performed using Nikon NIS-Elements Advanced Research (version 4.51; Nikon, Japan) and ImageJ software (National Institute of Health, NIH). Semi-automatic quantification of nuclear and cytoplasmic NF-κB p65 signals was carried out using a custom-designed plugin for the ImageJ software which is available on request. Data are based on three independent biological replicates, each performed with technical duplicates.

HPAIV Growth Kinetics

WT MEFs and MEFs with deleted importin-α3 or -α7 genes were infected with different multiplicities of infection (MOI) of SC35-PB2$_{701D}$ (H7N7, MOI 1 or 0.1) or SC35M-PB2$_{701N}$ virus (H7N7, MOI 0.01 or 0.001). 7*10^5 cells were inoculated with 2 mL virus dilution in DMEM (containing 1% P/S, 1% L-Glutamine, 1% NEAA, 1% sodium pyruvate) and incubated for 30 min at 5% CO_2, 96% rH and 37°C. After washing twice with acidic incubation medium (DMEM, pH 5.0, containing 1% FCS, 1% P/S, 1% L-Glutamine, 1% NEAA, 1% sodium pyruvate), 2 mL of pH-neutral incubation medium were added and the infected cells were incubated at 37°C. Virus titers of supernatants taken at 0, 24, 48, 72, and 96 hours post infection (p.i.) were determined as plaque forming units per ml (p.f.u./ml) by plaque assay [17] on MDCKII. For determination of importin-α protein levels after viral infection, WT MEFs were infected with SC35-PB2$_{701D}$ or SC35M-PB2$_{701N}$ virus at an MOI of 0.1. of WT MEF. Similarly, H1299 WT and H1299 with deleted importin-α3 gene were treated with TNFα (10ng/ml) 24h prior to inoculated with SC35M-PB2$_{701N}$ at MOI 0.001 (see above). TNFα treatment was re-applied and supernatant taken at 0, 24 and 48h p.i. Virus titers were determined by plaque assay on MDCK cells and given in p.f.u/ml. Additionally, primary human lung cells (HBEpC and HSAEpC) were infected with H5N1-PB2$_{701N}$ and H5N1-PB2$_{701D}$ (MOI = 0.1 and 1) or H7N7-PB2$_{627K}$ and H7N7-PB2$_{627E}$ (MOI = 1 and 10). Cells were lysed 24 and/or 48 hours p.i. in lysis buffer (50 mM HEPES (pH 8.0), 200 mM NaCl, 0.5% IGEPAL, 25% glycerol (Invitrogen), 1 mM PMSF, 0,07 μl/ml β-mercaptoethanol, 1x HALT Protease and Phosphatase Inhibitor Cocktail, 1x EDTA Solution (both: 100x, Pierce/Thermo Scientific). Whole cell protein extracts were subjected to western blot analysis.

Library Preparation and Next Generation Sequencing

Lungs of WT and α3$^{-/-}$ mice infected with 6*10^4 p.f.u. of SC35-PB2$_{701D}$ or SC35M-PB2$_{701N}$ (H7N7) were subjected to gene expression analysis. Control mice received PBS. On day 3 p.i., whole lungs were perfused, harvested and submerged in RNAlater and total RNA was isolated using the *innuprep* RNA Mini Kit (Analytik Jena). RNA samples from three animals per mouse strain and virus were pooled and used for gene expression analysis. For each sample, 1μg of total RNA was used for generating sequencing libraries with the Illumina TruSeq RNA Sample Preparation Kit v2 as recommended by the manufacturer (Illumina Inc.). Size and quality of

the libraries were visualized on a BioAnalyzer High Sensitivity DNA Chip (High Sensitivity DNA Kit, Agilent Technologies). Diluted libraries (2 nM) were multiplex-sequenced on the Illumina HiSeq 2500 instrument. For each sample between 78 and 113M, paired-end reads of 101 bp length were generated. The reads were aligned to the murine reference transcriptome (UCSC mm10) using Bowtie2 (v2.2.2) (Langmead and Salzberg, 2012). DESeq (Anders and Huber, 2010) was employed to assess differential expression based on read counts per gene. Genes were hierarchically clustered according to their expression profiles using the R function hclust (http://www.R-project.org/). DAVID (v6.7) (Huang et al., 2009) was employed to functionally annotate the resulting clusters. Networks of protein-protein interactions were computed and visualized using Cytoscape (Shannon et al., 2003).

TNF-α ELISA

TNF-α protein amount was determined in lung homogenate supernatants of WT mice infected intranasally with $6*10^4$ p.f.u. of SC35-$PB2_{701D}$ or SC35M-$PB2_{701N}$ viruses (H7N7). Whole lungs were harvested on day 1 p.i. and ~50–100 mg of tissue homogenized with ~300 μl glass beads (RETSCH #22.222.0003) in 1 mL 1x PBS (PAA) in the mixer mill MM400 (Retsch; 20 Hz, 4°C, 10 min). After centrifugation (6000 xg, 4°C, 5 min), lung homogenate supernatants were stored at −80°C. Supernatants of three animals per virus were pooled. Then, the Enzyme-linked Immunosorbent Assay (ELISA) Kit for murine TNF-α was performed according to the manufacturer's instructions (#E90133Mu, USCN Life Science Inc.).

TNF-α Treatment, Importin-α3 mRNA Expression, Subcellular Localization and Promoter Activation

HSAEpC, WT MEFs and $NEMO^{-/-}$ MEFs were seeded in 24-well plates until confluent or in 10 cm-dishes for 24 h, respectively, and serum starved for 24 h. Then, cells were control-treated (w/o) or treated with human TNF-α (50 ng/ml; #210-TA, R&D Systems) for 6 h or with murine TNF-α (50 ng/ml; #575204, BioLegend, Inc.) for 6 h or 24 h, respectively. WCL, CF, and NF were subjected to western blot analysis for importin-α3 and NF-κB p65 detection. Total RNA were isolated 6h post treatment for relative importin-α3 expression, using RT-qPCR.

For determination of the relative importin-α3 mRNA expression levels after cytokine treatment, $NEMO^{-/-}$ MEFs were seeded in 10cm cell culture dishes ($5x10^6$ cells per dish). After serum starvation for 24 h, cells were control-treated (mock) or treated 10 min with 10ng/ml of murine TNF-α, IL-6, IL-10, IFN-γ and TGF-β. After 6h post treatment, cells were harvested, RNA isolated and cDNA generated before RT-qPCR analysis.

For the determination of nuclear import of NF-κB p65 after TNF-α stimulation, WT MEF and Importin α3 KO MEF were seeded in 10cm cell culture dishes ($1x10^6$ cells per dish). After serum starvation for 18 h, cells were treated with 10ng/ml TNF-α. Subsequently, cells were harvested by scraping in ice-cold PBS, centrifuged and after removing the supernatant, the cells were resuspended in 50μl of Buffer A (10mM Tris pH7,9; 1,5mM $MgCl_2$; 10mM KCl). After adding 6μl of 2% NP-40 and vortexing, the samples were incubated for 10min on ice and centrifuged für 15min at 6,0000rpm at 4°C. The supernatant (cytosolic fraction) was placed in a fresh tube, subsequently the pellet was washed again with 100μl of buffer A, centrifuged again for 15min and the supernatant was removed. For nuclear fractions, the pellet was resuspended in 50 μl of buffer B (20 mM Tris pH 7.9; 10mM KCl; 1.5mM $MgCl_2$; 20% Glycerol) and vortexed; then 33 μl of buffer C (20mM Tris pH 7.9; 1.2M KCl; 1.5 mM $MgCl_2$; 20% Glycerol) was added and the samples were incubated on a wheel at 4°C for 45 min. Afterward, samples were centrifuged for 30 min at 12,000 rpm at 4°C and the supernatant (nuclear fraction) was transferred to a fresh reaction tube. Both fractions were mixed with 4x protein loading dye and boiled for 5 min at 95°C before being subjected to western blot analysis.

For determination of importin-a3 promoter activation in MEF cells, cells were seeded in 96-well plates (5000 cells/well) to reach approximately 60% confluency after 24h. Then, cells were transfected using FuGene HD transfection reagent (SwitchGear Genomics), either with pLightSwitch-Prom-Control (SwitchGear Genomics; 100 ng/well) as a control, or pLightSwitch-Prom-importin-α3 (SwitchGear Genomics; 100 ng/well) for importin-α3 promoter activity readout. After 24h, transfected cells were treated with murine TNF-α, IL-10 or TGF-β at 0, 1 or 50 ng/ml, for 15 min. Promoter activity was measured at 3h post treatment using LightSwitch™ Luciferase Assay Reagent (SwitchGear Genomics, LS010) according to manufacturer's instructions.

For determination of importin-α3 promoter activation, A549 or HSAEpC were seeded in 96-well plates for 24 h or until 80% confluency, respectively, and transfected with pLightSwitch_Prom-control (50 ng; Control) or pLightSwitch_Prom-importin-α3 (50 ng; α3) and pFL-TK (250 ng; firefly luciferase transfection control) using Lipofectamine-2000 or jetPRIME®, respectively. 14 h after transfection, serum starvation was initiated for 30 h. Subsequently, cells were treated with 0, 10, 50 or 100 ng/ml (A549) or with 0, 1, 10 or 100 ng/ml (HSAEpC) of human TNF-α and lysed 20 h later. Firefly and Renilla luciferase activities were assessed using the *Dual-Luciferase® Reporter Assay System* (Promega, E1910).

NEMO Complementation Assay

$NEMO^{-/-}$ MEFs were transfected in suspension with 5 μg empty vector pcDNA3.1 or pcDNA-HA-human NEMO in 6-well plates using Lipofectamine 2000 (Invitrogen) for 6 h. At 48 h post transfection, cells were serum starved for 24 h. Then, cells were control-treated (w/o) or treated with murine TNF-α (50 ng/ml; #575204, BioLegend, Inc.) for 6 h. WCL were subjected to western blot analysis for importin-α3 and NEMO detection.

QUANTIFICATION AND STATISTICAL ANALYSIS

P values of RT-qPCR data were obtained by Kruskal-Wallis one-way ANOVA using PAST v.2.17c (http://folk.uio.no/ohammer/past/). RT-qPCR data were considered as relevant when more than ± 1.5-fold change was detected in relative mRNA expression levels. Statistical significance of animal survival rates was determined with GraphPad Prism 5 v.5.03 (Graphpad Software, Inc.) using the Log Rank (Mantel-Cox) test and the Kaplan-Meier survival curves. All other mean values, standard deviations (SD), and P values were calculated with GraphPad Prism 5 (v5.03) or the GraphPad Software, Inc. tool (https://www.graphpad.com/quickcalcs/ttest1/?Format=SD) using the unpaired, two-tailed Student's t test or the one-sample, two-tailed Student's t test when all values in one group were identical, e.g., set 100%. Statistical significance was defined as $p < 0.05$ (* $p < 0.05$, ** $p < 0.01$, *** $p < 0.001$).

DATA AND CODE AVAILABILITY

Transcriptome sequence data reported in this publication is submitted to the European Nucleotide Archive (ENA) and is available under following link: https://www.ebi.ac.uk/ena/data/view/PRJEB8023.